Cell Reports
Methods

Article

# Efficiency landscape of bioorthogonal click reactions producing bispecific antibody conjugates

## Graphical abstract

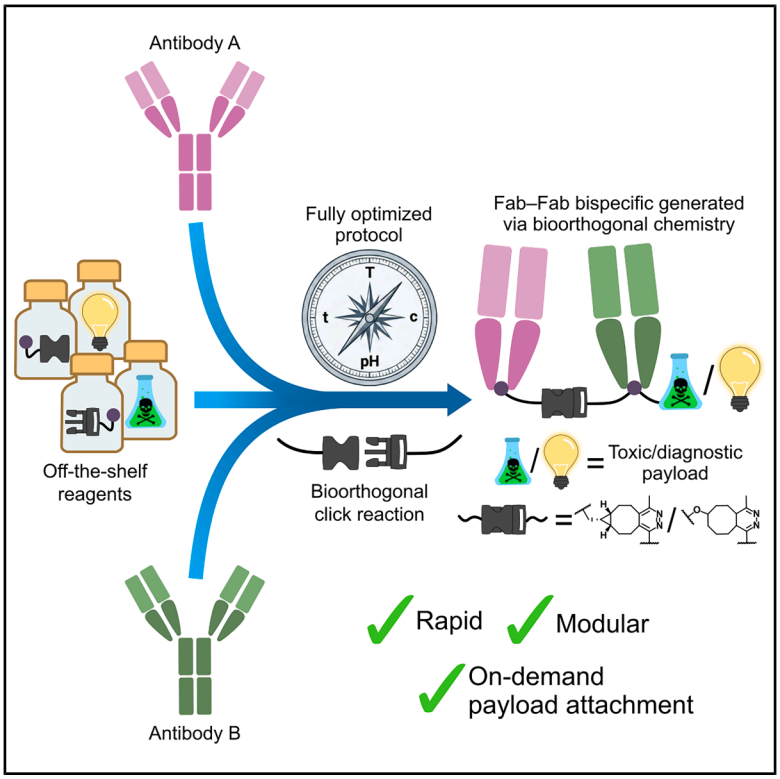


## Authors

László Petri, Írisz K. Kovács, Boglárka Szabó, ..., Vijay Chudasama, Peter A. Szijj, György M. Keserű

## Correspondence

pszijj@stanford.edu (P.A.S.), keseru.gyorgy@ttk.hu (G.M.K.)

## In brief

Bispecific antibodies can bind to multiple targets simultaneously and have been increasingly successful in oncology. However, traditional methods for their generation are resource intensive. Petri et al. report optimization of chemical assembly of bispecific antibodies, offering a rapid and modular alternative using commercially available components.

## Highlights

- Systematic analysis of two chemical approaches for bispecific antibody production
- Design of experiments framework for reaction parameters
- Modular and rapid method that relies exclusively on off-the-shelf reagents

Petri et al., 2026, Cell Reports Methods 6, 101416
June 15, 2026 
https://doi.org/10.1016/j.crmeth.2026.101416

CellPress

Cell Reports Methods

CellPress
OPEN ACCESS

Article

# Efficiency landscape of bioorthogonal click reactions producing bispecific antibody conjugates

László Petri,[1,2] Írisz K. Kovács,[1,2,3] Boglárka Szabó,[1,2,3] Tímea Imre,[1,2,4] Anita Rácz,[2,5] Vijay Chudasama,[6] Peter A. Szijj,[6,7,*] and György M. Keserű[1,2,3,8,*]

[1]Medicinal Chemistry Research Group, HUN-REN Research Centre for Natural Sciences, 2 Magyar tudósok krt, 1117 Budapest, Hungary
[2]National Drug Discovery and Development Laboratory, HUN-REN Research Centre for Natural Sciences, 2 Magyar tudósok krt, 1117 Budapest, Hungary
[3]Department of Organic Chemistry and Technology, Budapest University of Technology and Economics, 4 Szt. Gellért tér, 1111 Budapest, Hungary
[4]MS Metabolomics Research Laboratory, HUN-REN Research Centre for Natural Sciences, 2 Magyar tudósok krt, 1117 Budapest, Hungary
[5]Plasma Chemistry Research Group, HUN-REN Research Centre for Natural Sciences, 2 Magyar tudósok krt, 1117 Budapest, Hungary
[6]Department of Chemistry, University College London, 20 Gordon Street, London WC1H OAJ, UK
[7]Stanford Sarafan ChEM-H and Department of Chemistry, Stanford University, Stanford, CA 94305, USA
[8]Lead contact
*Correspondence: pszijj@stanford.edu (P.A.S.), keseru.gyorgy@ttk.hu (G.M.K.)
https://doi.org/10.1016/j.crmeth.2026.101416

**MOTIVATION** The field of bispecific antibody generation has traditionally been dominated by the expression of fusion proteins, a class of methods heavily optimized over the past 30 years. Competitive chemical methods have only recently begun emerging and are yet to be optimized to any comparable extent, making their wide-scale adoption difficult. Our manuscript addresses this unmet need by providing a detailed reactivity landscape for the chemical assembly of antibody fragments using IEDDA reactions.

## SUMMARY

Bioorthogonal conjugation techniques offer a powerful and flexible approach for the modular construction of multifunctional biomolecules, such as bispecific antibodies. In this study, we systematically compared two inverse electron demand Diels-Alder (IEDDA) reactions, between tetrazine and either *trans*-cyclooctene (TCO) or bicyclo[6.1.0]nonyne (BCN), to generate chemically conjugated bispecific antibody constructs. We applied a design of experiments (DoE) framework to explore how various reaction parameters influence conjugation efficiency. The two systems exhibited distinct reactivity patterns: the BCN-tetrazine reaction proved to be more robust, while the TCO-tetrazine ligation showed a more complex dependency on reaction time and temperature. To assess biological functionality, the bispecific constructs were evaluated by ELISA, confirming preserved antigen-recognition after both conjugation strategies. Both strategies consistently yielded bispecific constructs with comparable physicochemical and functional profiles. These insights support the application of this chemical conjugation strategy as a rapid, tunable, and modular platform for early-stage multispecific antibody development.

## INTRODUCTION

Cancer remains one of the most pressing global health challenges, responsible for one in six deaths according to WHO data.[1] Mortality rates continue to rise globally, emphasizing the high unmet need for improved and more precisely targeted treatment strategies. Over the past two decades, advances in diagnostics and therapeutic modalities, particularly antibody-based biologics, have revolutionized cancer therapy.[2–6] Antibody-drug conjugates (ADCs) and bispecific antibodies (bsAbs) have emerged as powerful tools in the oncologist's toolkit, offering targeted delivery of potent cytotoxins and targeted immune activation, enhanced selectivity over conventional antibodies, or enhanced internalization by co-targeting a highly trafficked receptor, respectively.[7–12] Bispecific antibody-drug conjugates (bsADCs)[13] aim to combine these functionalities, providing enhanced delivery of the toxic payload compared to conventional ADCs. However, their clinical translation has been held back by a laborious manufacturing process. Traditional production of bsAbs and related constructs[14–22] relies on complex protein engineering and mammalian cell expression, posing challenges in scalability, cost, and chain-pairing fidelity.[23] In

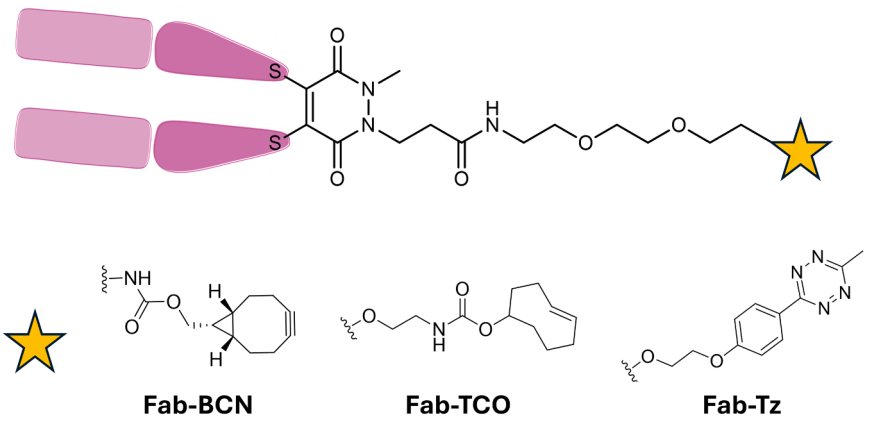


**Figure 1. Design of Fab derivatives used in Fab-Fab crosslinking experiments**

The scheme shows Fab-BCN, Fab-TCO, and Fab-Tz constructs, generated via $Br_2$PD-based disulfide rebridging.

response, bioorthogonal click chemistry has gained prominence as a powerful, modular alternative, offering high specificity, rapid kinetics, and compatibility with aqueous conditions. This class of reactions, recognized by the 2022 Nobel Prize in Chemistry, enables the selective functionalization of biomolecules under mild conditions,[24] making it especially valuable for constructing bsAbs, ADCs, and bsADCs. Systematic investigation of the stability and orthogonality of click handles has been recently reported, concluding that even widely regarded "bioorthogonal" functionalities may suffer from hydrolysis, redox sensitivity, or unintended cross-reactivity in multistep workflows.[25] These insights are particularly relevant in the context of antibody modification, where reducing agents or specific buffer components may compromise the efficiency of conjugation.

Fab-Fab constructs are a class of bispecific antibodies, that, similarly to other fragment-based formats such as BiTEs, DARTs, and tandem scFvs, possess no Fc component.[26] The study we present herein centers on the chemical assembly of $Fab_2$-type bispecific antibody constructs using two inverse electron-demand Diels-Alder (IEDDA) ligation systems: the classical IEDDA reaction involving *trans*-cyclooctene (TCO) and its alternative; bicyclononyne (BCN) with tetrazine. These ligations offer biocompatibility and are among the fastest known bioorthogonal reactions,[27–29] forming stable pyridazine or dihydropyridazine products. Click chemistry-based chemical conjugation offers several advantages over recombinant bsAb expression.[30] These modular approaches enable precise control over conjugation stoichiometry and site, avoid chain mispairing, and allow easy diversification with small molecule cargo. Moreover, chemical assembly can be scaled rapidly, suiting both preclinical development and personalized medicine applications. Our goal was to optimize these ligation strategies and evaluate the physicochemical properties of the resulting bispecific antibodies.

Combining advances in the fields of bioconjugation, antibody engineering, and click chemistry enables access to diverse molecules and functions hard to access via other means. Constructs such as multispecific checkpoint inhibitory T cell engagers (CiTEs) and bsADCs exemplify cutting-edge developments enabled by combining these approaches.[31] With an increasing number of bsADCs entering clinical trials, there is a clear demand for scalable and robust ways of generating these biologics. Our findings contribute to these efforts and demonstrate that chemical conjugation of $Fab_2$-type bsAbs and bsADCs utilizing optimized BCN and TCO IEDDA ligations are not only feasible but potentially superior in flexibility and cost-efficiency over expression-based production. In this study, we intended to provide a comprehensive chemical framework for producing bispecific antibody-based therapeutics using bioorthogonal click chemistry that might be useful for translating the promise of personalized immunotherapy into widespread clinical practice.

## RESULTS AND DISCUSSION

The systematic assessment of TCO and BCN-based ligation involved a full-factorial design of experiments (DoE) approach that explores the impact of key variables on ligation efficiency, including concentration, pH, reaction time, and temperature. We also compared the stoichiometric requirements of TCO- and BCN-derived constructs to aid cost-effective production. Next, the antigen targeting capabilities of the resulting $Fab_2$-conjugates were validated by ELISA, confirming unaffected recognition of HER2 and CD20 epitopes.

### Scientific approach

Fragment antigen-binding (Fab) units represent advantageous antibody-derived platforms that retain high-affinity and selective antigen recognition, while providing a technically tractable and well-defined format for controlled site-specific chemical functionalization and subsequent protein-protein conjugation.[32–36] Unlike full-length IgGs that contain multiple interchain disulfide bonds across their heavy and light chains, each Fab contains a single, conserved interchain disulfide bridge between its constant regions.[37] This architectural simplicity renders Fabs amenable to controlled chemical manipulation: selective reduction of the sole disulfide bridge liberates two reactive nucleophilic thiol groups, which can be rebridged with a suitable dually reactive electrophile. In this manner, a single molecule can be inserted per Fab, allowing for tight control of the number and type of functional handles installed per protein unit. Consequently, Fabs offer an ideal starting point for generating defined antibody conjugates and bispecific constructs. Taking advantage of this, and building on previous work,[30,38–42] we generated disulfide-rebridged Fab derivatives bearing orthogonal click handles to serve as building blocks for bsAb-assembly. Our synthetic efforts focused on preparing three distinct Fab formats: Fab×TCO, Fab×BCN, and Fab×Tz (each harboring a unique click-reactive moiety: *trans*-cyclooctene, bicyclo[6.1.0]non-4-yne, or tetrazine, respectively) that enables subsequent rapid coupling under catalyst-free conditions (Figures 1 and S1).

CellPress
OPEN ACCESS

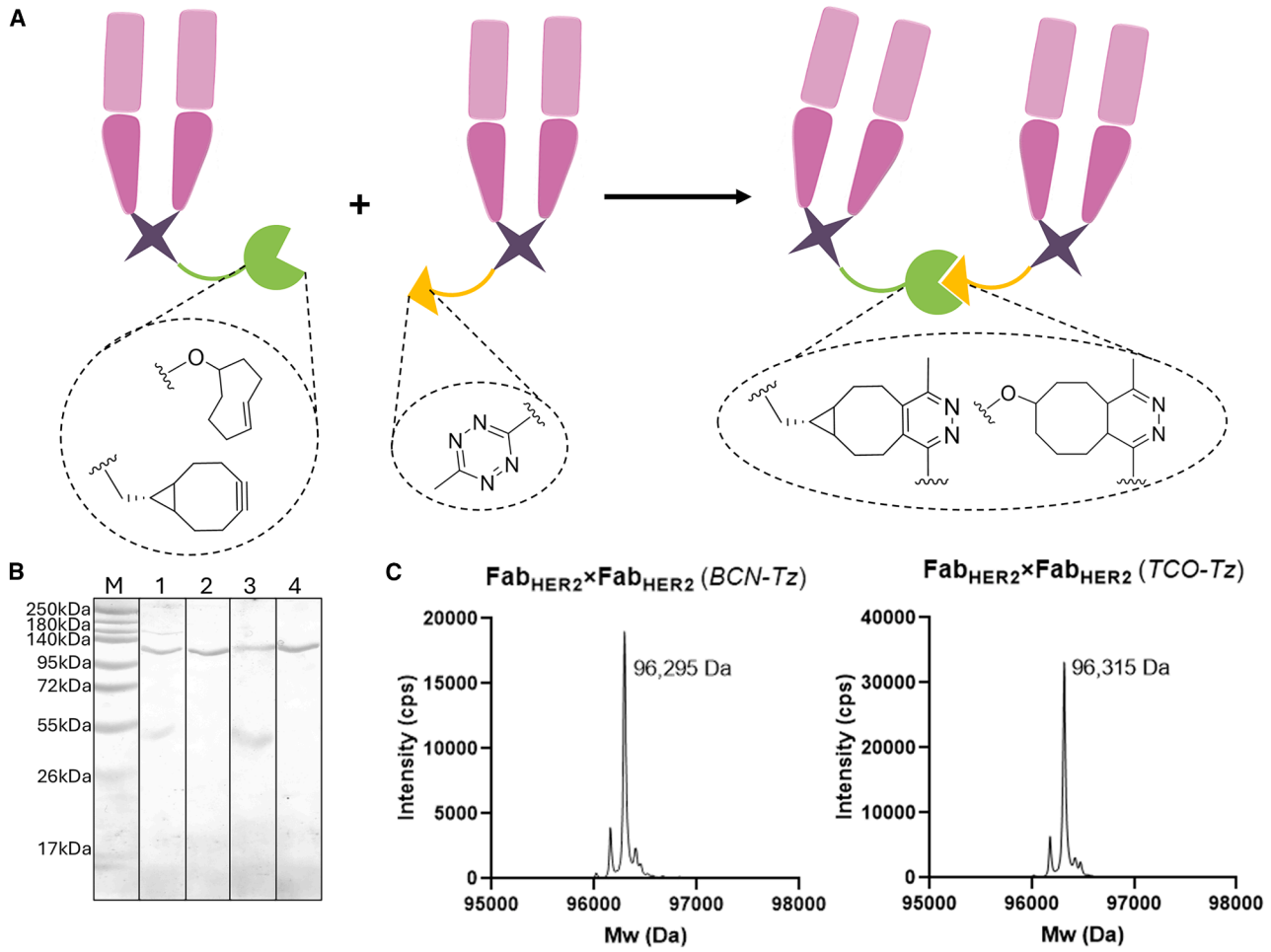


**Figure 2. General scheme of Fab-Fab crosslinking reactions and analytical characterization of the conjugates**

(A) General scheme of bioconjugation reaction to generate $Fab_{HER2}$×$Fab_{HER2}$ constructs.

(B) SDS-PAGE, where the lanes are M: protein marker, 1: crude $Fab_2$ product made of Fab×BCN, 2: SEC-purified $Fab_2$-type product made of Fab×BCN, 3: crude $Fab_2$ product made with Fab×TCO, 4: SEC-purified $Fab_2$ product made with Fab×TCO.

(C) Mass spectrometry results showing the mass of the produced $Fab_{HER2}$×$Fab_{HER2}$ constructs.

In this approach, controlled functionalization of Fabs is enabled by reduction and rebridging of the interchain disulfide bond. We employed tris(2-carboxyethyl)phosphine (TCEP) as a mild, thiol-specific reducing agent at a 50-fold molar excess for 1.5 h at 37°C. This condition efficiently liberated the two free thiol groups. After reduction, Fab proteins were reacted with the $Br_2$PD-based rebridging agents (Figure 1), enabling re-formation of the covalent linkage between the heavy and light chains of the Fab alongside installation of a click handle. All conjugations (Figure 1) were monitored by SDS-PAGE, and products were confirmed by electrospray ionization mass spectrometry (ESI-MS) measurements, with excellent agreement between calculated and observed masses for all Fab conjugates.

## Reactivity landscape

To enable reliable interpretation of the optimization experiments, we first established a $Fab_2$ reference standard (Figure 2). Fab×BCN or Fab×TCO constructs were reacted in a 1:1 molar ratio with Fab×Tz in PBS (pH 7.4) and incubated overnight under argon at 37°C. The resulting $Fab_2$ conjugates were purified by size-exclusion chromatography (SEC), and the collected fractions were analyzed by SDS-PAGE and mass spectrometry (Figure 2). The MS data confirmed the expected masses for the ligated $Fab_2$ products made with both Fab×BCN (calculated: 96,295 Da; found: 96,295 Da) and Fab×TCO (calculated: 96,315 Da; found: 96,315 Da), validating these constructs as reliable external standards for subsequent quantification.

Next, to investigate the influence of reaction conditions on conjugation efficiency, we employed a $2^4$ full factorial experimental design with five center points assessing the effects of temperature, pH, reaction time, and initial concentration. Protein-protein conjugation efficacy was estimated as MS-quantified yield of the $Fab_2$ products (Tables 1 and S1). To enable accurate and reproducible quantification, samples were supplemented with unconjugated Fab as an internal standard. As described above, purified $Fab_2$ product was used as an external

**Table 1. DoE matrix listing the tested parameters for Fab-Fab ligation reactions**

| Experiment | *c* (μM) | *T* (°C) | pH | *t* (h) | Yield of BCN-Tz reaction (%) | Yield of TCO-Tz reaction (%) |
|---|---|---|---|---|---|---|
| 1 | 20 | 4 | 5 | 1 | 12 | 35 |
| 2 | 20 | 37 | 5 | 1 | 24 | 54 |
| 3 | 20 | 4 | 9 | 1 | 13 | 34 |
| 4 | 20 | 37 | 9 | 1 | 23 | 52 |
| 5 | 20 | 4 | 5 | 16 | 71 | 60 |
| 6 | 20 | 37 | 5 | 16 | 58 | 57 |
| 7 | 20 | 4 | 9 | 16 | 61 | 70 |
| 8 | 20 | 37 | 9 | 16 | 28 | 25 |
| 9 | 100 | 4 | 5 | 1 | 80 | 70 |
| 10 | 100 | 37 | 5 | 1 | 83 | 80 |
| 11 | 100 | 4 | 9 | 1 | 72 | 58 |
| 12 | 100 | 37 | 9 | 1 | 85 | 63 |
| 13 | 100 | 4 | 5 | 16 | 87 | 85 |
| 14 | 100 | 37 | 5 | 16 | 84 | 61 |
| 15 | 100 | 4 | 9 | 16 | 47 | 59 |
| 16 | 100 | 37 | 9 | 16 | 39 | 36 |
| 17 | 60 | 20.5 | 7 | 8.5 | 58 | 66 |
| 18 | 60 | 20.5 | 7 | 8.5 | 68 | 68 |
| 19 | 60 | 20.5 | 7 | 8.5 | 65 | 79 |
| 20 | 60 | 20.5 | 7 | 8.5 | 51 | 70 |
| 21 | 60 | 20.5 | 7 | 8.5 | 61 | 75 |

Conditions include concentration (*c*), temperature (*T*), pH, and reaction time (*t*). Corresponding conjugation efficacy (yield) for both BCN- and TCO-based crosslinking reactions are also reported for each condition.

reference. This was defined as 100% yield. The reactions were then analyzed under identical LC-MS conditions and the ratio of the $Fab_2$ MS signal intensity to that of the external reference was calculated to determine the yield of the protein-protein conjugation. For each reaction, the yield was defined as the relative amount of $Fab_2$ formed under the given conditions, expressed as a percentage of the theoretical maximum (100% reaction efficacy).

The full factorial design revealed the significant effects of concentration, pH, and time, as well as the notable interactions involving temperature (Table S2). Replicates at the center point showed good reproducibility, with yields of 60.6 ± 6.6% and 71.8 ± 5.5% for the BCN and TCO series, respectively. The highest yield for the BCN-based ligation technique was obtained under mild acidic conditions (pH 5) and high initial concentrations (100 μM), especially at lower temperatures (4°C–20°C). Interestingly, temperature alone did not significantly impact the yield ($p$ = 0.575), indicating that BCN-Tz reactivity is relatively robust across the tested temperature range. Graphical representation of the parameter space (Figure 3A) highlighted a clear preference for lower pH and higher reactant concentrations, providing a rational basis for selecting optimal conditions.

For the TCO-Tz-based IEDDA reactions, similar analysis revealed a more complex reactivity pattern (Figure 3B). In addition to pH and concentration, statistically significant interaction was observed between temperature and time ($p$ = 0.0112; Table S2) suggesting kinetic control under certain conditions. Specifically, short reaction times at elevated temperatures, and prolonged incubations at low temperatures both resulted in high yields. These trends were visualized in Figure 3B indicating strong temperature-time dependency as a distinctive feature compared to the BCN-Tz system. As with BCN-Tz reactions, acidic conditions (pH 5) and high reactant concentrations (100 μM) promoted product formation.

When comparing the click reactions directly, we found no statistically significant difference in the achievable yields under the optimized conditions (Figure 4). A Kolmogorov-Smirnov test further confirmed this equivalence ($p$ = 0.718). The temperature and pH dependencies followed nearly identical trends, and neither concentration nor time alone influenced the yields significantly. The only practical distinction was the temperature-time interaction in TCO-Tz reactions, requiring tailored optimization depending on thermal and temporal constraints. However, since both systems performed best at lower temperatures (4°C–20°C), this does not influence their synthetic utility. Overall, both click strategies provide robust and tunable platforms for Fab-Fab conjugate formation under mild conditions.

To further optimize the click conjugation reactions, we systematically investigated the effect of the molar ratio of the reactants by varying the equivalents of BCN or TCO relative to the tetrazine-modified counterpart (Figure 5; Table S3). Reactions were performed using 0.5, 0.9, 1.0, 1.1, or 1.5 equivalents of the dienophile (BCN/TCO) partner. In the case of the BCN-tetrazine ligation, we observed that a slight excess of the Fab-Tz moiety (particularly 1.1 eq. Fab-Tz) resulted in the highest yield (87 ± 7%). This finding is consistent with the previous observations[30] that confirmed the benefit of a slight molar excess of the tetrazine. In contrast, for the TCO-Tz ligation, we found that equimolar amounts (1:1) of Fab-TCO and Fab-Tz provided optimal conjugation (86 ± 12%), with no significant improvement upon the addition of excess Fab-Tz. This difference likely reflects the inherently faster kinetics and higher reactivity of the TCO-Tz IEDDA reaction, which proceeds efficiently without requiring an excess of either component. These findings emphasize the importance of fine-tuning the stoichiometry of reactants based on the specific click partners used, and they provide practical guidance for efficient bioconjugation setup.

### *Product feature landscape*

Using our optimized conditions, we set out to produce bsAb-dye conjugates to exemplify the utility of our method. We performed a two-step, one-pot procedure (Figure 6A) using a dibenzocyclooctyne (DBCO) containing click-enabled TAMRA dye and a dual-reactive Fab ($Fab_{CD20}$×Tz-$N_3$) alongside either $Fab_{HER2}$×BCN or $Fab_{HER2}$×TCO. TAMRA-DBCO would then react with the $N_3$ click handle in an orthogonal fashion to the IEDDA reactions between Tz and BCN or TCO to generate $Fab_{HER2}$×$Fab_{CD20}$×TAMRA conjugates. To understand the functional and analytical profile of the chemically constructed bsAb-dye conjugates, we thoroughly characterized the $Fab_{HER2}$×$Fab_{CD20}$×TAMRA constructs (Figure 6) in terms of purity, integrity, and target-specific binding affinity using a combination of methods. Following the reaction, the crude conjugation mixture contained some residual components (unreacted Fab

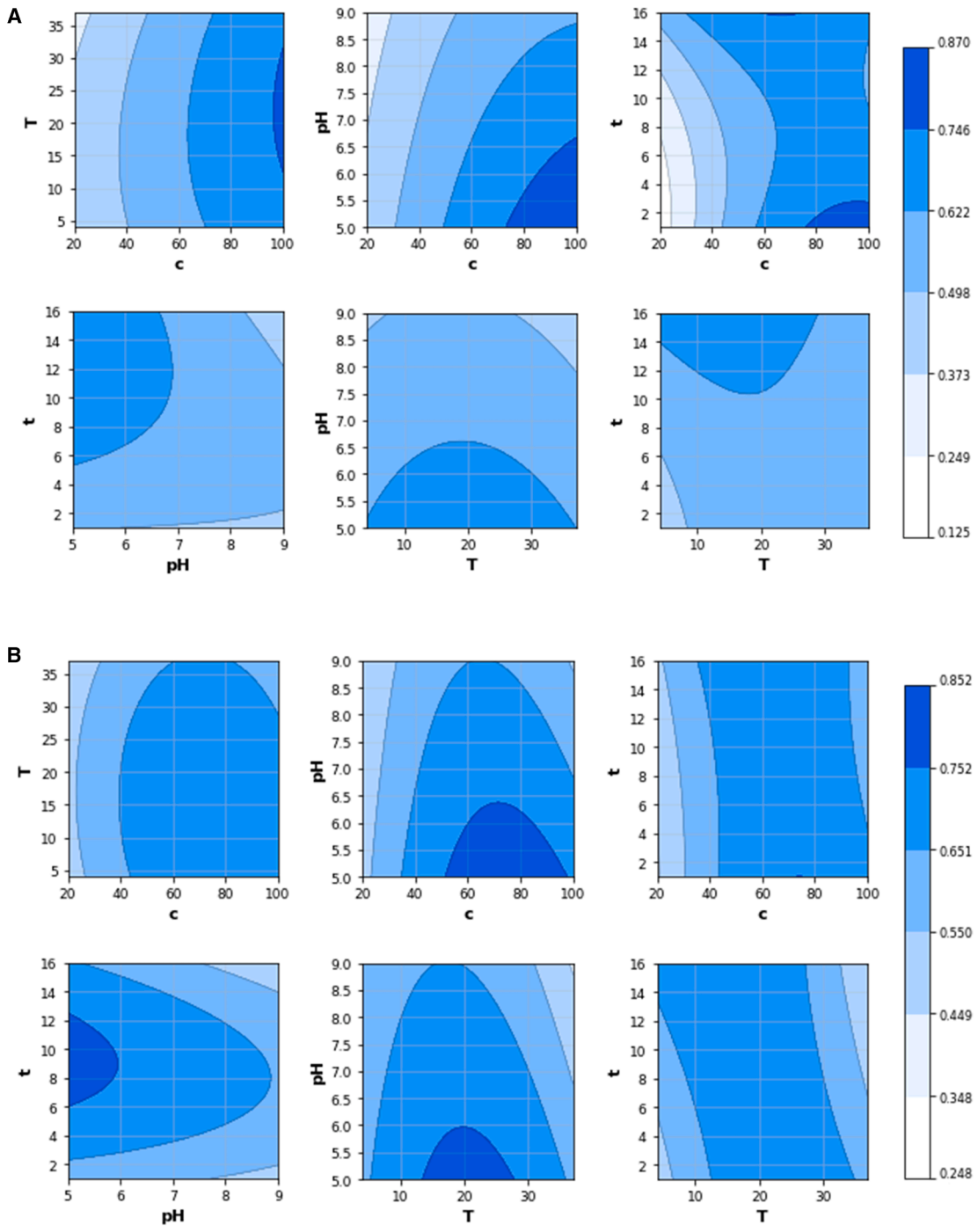


**Figure 3. Probability surface plots of full factorial DoE for Fab-Fab crosslinking**

(A) BCN-Tz-based IEDDA reaction and (B) TCO-Tz-based IEDDA reaction. Yield is color-coded from light blue (low) to dark blue (high).

precursors and small molecules), which necessitated purification. SEC was employed to isolate the pure bsAb-fluorophore conjugates, followed by sample concentration adjustment and protein quantification by the Bradford assay. The conjugates were subsequently validated by SDS-PAGE using both Coomassie Brilliant Blue (CBB) staining and fluorescence detection (Figure 6B), and mass spectrometry (Figure 6C), supporting the molecular identity of the $Fab_{HER2}\times Fab_{CD20}\times$TAMRA conjugates. An in-source neutral loss of water (−18 Da) was consistently observed in both the BCN-ligated product (calculated: 97,167 Da; found: 97,148 Da) and the TCO-ligated product (calculated: 97,187 Da; found: 97,166 Da). With the optimized protocol, we

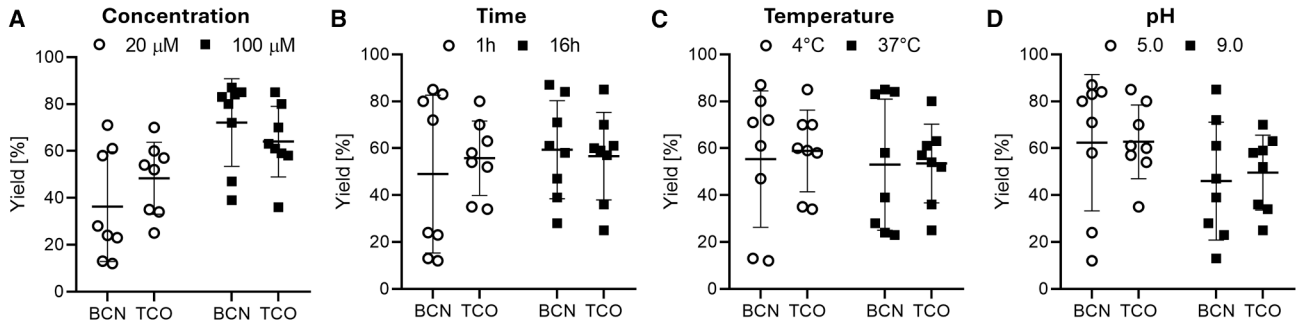


**Figure 4. Head-to-head comparison of BCN- and TCO-based ligations under different reaction conditions**

Parameters include concentration (A), time (B), temperature (C), and pH (D). Data represent $n = 8$ distinct experimental conditions (with no technical replicates) corresponding to all parameter combinations grouped by the indicated level of concentration (A), time (B), temperature (C), or pH (D), and shown with the SD of the group.

were able to obtain the $Fab_{HER2}$×$Fab_{CD20}$×TAMRA constructs after SEC purification in 61% and 68% isolated yields for BCN-Tz and TCO-Tz click reactions, respectively. Similarly, the described two-step, one-pot procedure provided $Fab_{HER2}$-$Fab_{EGFR}$-MMAE bispecific antibody-drug conjugates in 57% and 65% isolated yields for BCN-Tz and TCO-Tz click reactions, respectively (Figures S2). These results strongly demonstrate the broad applicability and modularity of the extensively optimized conjugation platform for producing series of bispecific constructs with varied antibody and payload components.

Next, the physicochemical stability of the $Fab_{HER2}$×$Fab_{CD20}$×TAMRA conjugates was systematically evaluated under different storage and *in vivo*-like conditions. Conjugates were incubated in phosphate-buffered saline (PBS, pH 7.4) at 4°C or in fetal bovine serum (FBS) at 37°C over different time intervals (1 week and 1 day, respectively). The integrity of the conjugates was monitored by SDS-PAGE with both standard CBB staining and fluorescent visualization (Figure S3). Gels consistently showed intact, homogeneous Fab-Fab conjugates across all time points. These results demonstrate that the optimized conjugates are highly stable under conditions relevant to both storage and biological application, supporting the robustness and practical utility of the optimized IEDDA-based conjugation platform discussed in this study.

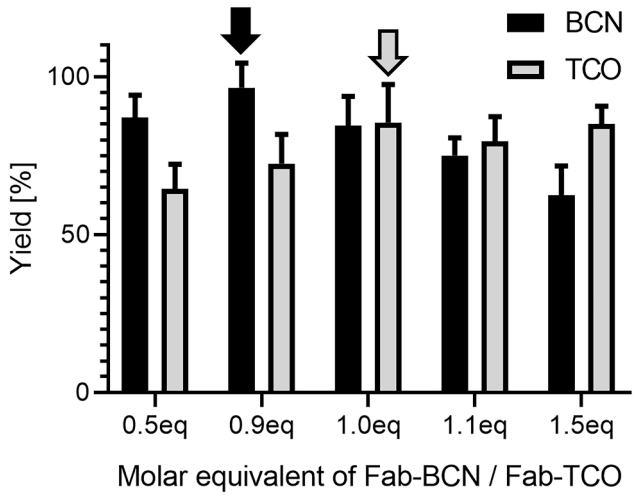


**Figure 5. Optimization of molar equivalents applied in conjugation reactions**

Yields are shown as means of duplicates and corrected to the theoretical maximum in each condition tested. Equivalents are calculated for Fab×BCN or Fab×TCO reagents over Fab×Tz reagent. Arrows are pinpointing the highest yields. Results are shown as mean with SD, $N = 2$ biological replicates are shown in each group.

The binding performance of the fluorescent bispecific antibody conjugates was then assessed by ELISA assay measurements (Figure S4). After immobilization of the antigens and blocking the wells with BSA, serial dilutions of purified $Fab_{HER2}$×$Fab_{CD20}$×TAMRA conjugates were applied to assess antigen recognition capacity. Detection was performed using horseradish peroxidase (HRP)-conjugated anti-Fab secondary antibodies and a colorimetric readout at 450 nm. Both HER2- and CD20-specific Fab arms retained their antigen binding capabilities in linked constructs, with no significant difference observed as compared to the unconjugated parent Fabs. For BCN-Tz conjugated products, this is consistent with previous findings reported by Maruani et al.,[30] while importantly, we also demonstrated herein that the same holds true for TCO-Tz conjugation. Moreover, no recognition interference was detected between the two Fab moieties within the bispecific construct, indicating that antigen recognition was not compromised by mutual structural or steric hindrance. These results collectively confirm that the chemical conjugation strategy preserves target specificity and dual binding functionality after both investigated bioorthogonal click reactions.

Finally, we carried out hydrophobic interaction chromatography (HIC) analysis of the $Fab_{HER2}$×$Fab_{HER2}$ constructs (Figure S5) to assess their developability. Gratifyingly, HIC analysis of the chemically generated $Fab_2$ constructs revealed increased hydrophilicity of the chemically linked $Fab_2$ constructs (with Rt of 10.9 and 11.1 min related to the BCN- and TCO-based conjugated bispecifics, respectively) as compared to $F(ab')_2$, their native structural analogue (with Rt of 13.9 min). Attachment of hydrophobic payloads can lead to a loss of solubility and increase in aggregation, a well-established effect in antibody-drug conjugate development, where HIC is routinely employed to monitor drug-induced hydrophobicity changes.[43] Consequently,

CellPress
OPEN ACCESS

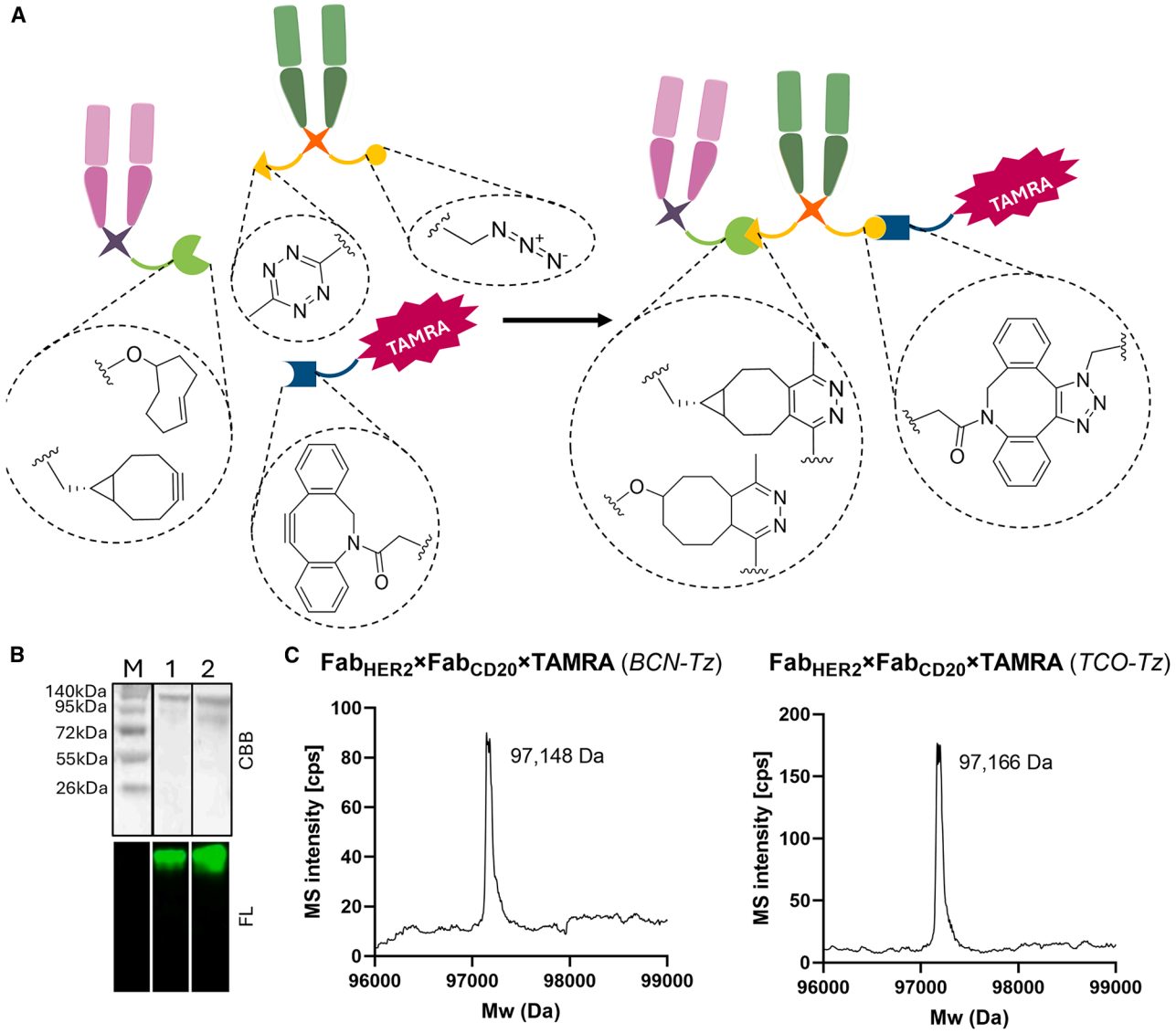


**Figure 6. Schematic overview of Fab$_{HER2}$× Fab$_{CD20}$×TAMRA conjugate assembly, linking rituximab (orange) and trastuzumab (purple) Fabs with a TAMRA fluorescent dye (magenta dodecagram)**

(A) General scheme.

(B) Product analysis by SDS-PAGE, where fluorescence (FL) readout and CBB-stained SDS-PAGE gels are shown as M: protein marker, 1: SEC-purified Fab$_{HER2}$×Fab$_{CD20}$×TAMRA conjugate made with Fab×BCN, 2: SEC-purified Fab$_{HER2}$×Fab$_{CD20}$×TAMRA conjugate made with Fab×TCO.

(C) Mass spectrometry results showing the mass of the produced Fab$_{HER2}$× Fab$_{CD20}$×TAMRA constructs.

the increase in hydrophilicity associated with the conjugation chemistry is expected to partially offset the challenges inherent to the attachment of hydrophobic payloads, leading to improved physicochemical properties for the constructs.

As demonstrated herein, we have successfully carried out an in-depth methodological optimization of IEDDA click chemistry-based bispecific antibody-assembly, exploring the impact of key reaction parameters (pH, temperature, time, and concentration). We then used the optimized reaction conditions to demonstrate the generation of model bsAb conjugates with both BCN-Tz and TCO-Tz reactions. Fab$_{HER2}$×Fab$_{CD20}$×TAMRA and Fab$_{HER2}$×Fab$_{EGFR}$×MMAE were afforded rapidly (within 5 days starting from the parental monoclonal antibodies including enzymatic digestion, chemical modification, and chromatographic purification of the final bispecific construct), and in good isolated yield (57%–68%). The conjugate was shown to retain binding of both Fab components to their respective antigens via ELISA. Moreover, Thoreau and colleagues have recently demonstrated[44,45] that similar rebridging strategies can be applied to the Fc region and full-length antibodies without compromising the efficiency of subsequent IEDDA reactions. These studies show that the click reactivities remain broadly comparable across

Fab, Fc, and full-length mAb constructs, supporting the general applicability of the method optimized herein, even beyond linkage of Fab fragments. Thus, we believe this optimization work opens the door to chemistry-focused laboratories to start research programs based on the generation of protein-protein conjugates. All the required components are commercially available, and the method has now been thoroughly optimized. We invite fellow chemical biologists who have held back from generating multiprotein constructs due to reservations about expression-based methods and their inherent difficulties, to explore chemical protein-protein conjugation as an alternative strategy. The temporal and financial investment to make biologically relevant multifunctional molecules has never been lower.

### Limitations of the study

The bispecific antibody constructs generated and appraised in this study lack an Fc component and would therefore have shorter serum half-lives *in vivo*, due to a lack of FcRn-mediated recycling. This would necessitate repeated dosing in a clinical setting. The BCN/tetrazine IEDDA method has previously been demonstrated for the generation of Fc-containing IgG-like bispecific synthetic antibodies (SynAbs); therefore, the condition-optimization reported here is expected to be transferrable to that context. Regardless, future work should optimize the generation of SynAbs and SynAb-small molecule conjugates in an analogous manner to the DoE analysis carried out here. It would likewise be beneficial to appraise the *in vivo* pharmacokinetics and anti-cancer activity of the $Fab_2$ bispecifics reported here compared to Fc-containing SynAbs and conventional mAbs.

## RESOURCE AVAILABILITY

### Lead contact

Requests for further information and resources should be directed to and will be fulfilled by the lead contact, György M. Keserű (keseru.gyorgy@ttk.hu).

### Materials availability

All unique/stable reagents generated in this study are available from the lead contact with a completed materials transfer agreement.

### Data and code availability

- This paper does not report custom code.
- Raw and analyzed data (HPLC-MS and NMR spectra) are accessible in the supplementary information on Mendeley Data: https://doi.org/10.17632/xx6zczcxzm.1
- Any additional information required to reanalyze the data reported in this paper is available from the lead contact upon request.

## ACKNOWLEDGMENTS

We are grateful to everyone who has supported this work thus far. We thank A. Maruani for his insightful input on the results and T. Takács for assistance with SEC purification. This work was supported by the PharmaLab RRF-2.3.1-21-2022-00015, as well as the PD124598 and SNN151010 grants from the National Office of Research, Innovation and Technology. A.R. was supported by the Hungarian Academy of Sciences: János Bolyai Research Scholarship.

## AUTHOR CONTRIBUTIONS

L.P., P.A.S., and G.M.K. created the scientific research concept and acquired financial sources; L.P. and I.K.K. designed the experiments; L.P., I.K.K., and B.S. conducted chemical biology experiments; A.R. performed DOE analysis; T.I. did MS measurements; and L.P., P.A.S., V.C., and G.M.K. prepared the manuscript and guided the project.

## DECLARATION OF INTERESTS

The authors declare no competing interests.

## DECLARATION OF GENERATIVE AI AND AI-ASSISTED TECHNOLOGIES IN THE WRITING PROCESS

Generative AI tools were not used for data analysis or writing the original draft of the manuscript. During the preparation of the manuscript, OpenAI's GPT-4o LLM was utilized in some instances, exclusively to refine and improve the clarity and readability of the text. The authors carefully reviewed and extensively edited all content and take full responsibility for the final version of the manuscript.

## STAR★METHODS

Detailed methods are provided in the online version of this paper and include the following:



## SUPPLEMENTAL INFORMATION

Supplemental information can be found online at https://doi.org/10.1016/j.crmeth.2026.101416.

Received: November 18, 2025
Revised: February 18, 2026
Accepted: March 24, 2026
Published: April 21, 2026

## REFERENCES

1. Ferlay, J., Colombet, M., Soerjomataram, I., Parkin, D.M., Piñeros, M., Znaor, A., and Bray, F. (2021). Cancer statistics for the year 2020: An overview. Int. J. Cancer *149*, 778–789. https://doi.org/10.1002/ijc.33588.
2. Padma, V.V. (2015). An overview of targeted cancer therapy. Biomedicine *5*, 19. https://doi.org/10.7603/s40681-015-0019-4.

3. Papież, M.A., and Krzyściak, W. (2021). Biological Therapies in the Treatment of Cancer—Update and New Directions. Int. J. Mol. Sci. *22*, 11694. https://doi.org/10.3390/ijms222111694.

4. Kazemi, T., Younesi, V., Jadidi-Niaragh, F., and Yousefi, M. (2016). Immunotherapeutic approaches for cancer therapy: An updated review. Artif. Cells, Nanomed. Biotechnol. *44*, 769–779. https://doi.org/10.3109/21691401.2015.1019669.

5. Zhong, H.-J., Zhen, Y., Chen, S., Shi, W., Liang, X., and Yang, G.-J. (2025). Advances in CTC and ctDNA detection techniques: opportunities for improving breast cancer care. Breast Cancer Res. *27*, 97. https://doi.org/10.1186/s13058-025-02024-7.

6. Urruticoechea, A., Alemany, R., Balart, J., Villanueva, A., Viñals, F., and Capellá, G. (2010). Recent Advances in Cancer Therapy: An Overview. Curr. Pharm. Des. *16*, 3–10. https://doi.org/10.2174/138161210789941847.

7. Kontermann, R.E. (2012). Dual targeting strategies with bispecific antibodies. mAbs *4*, 182–197. https://doi.org/10.4161/mabs.4.2.19000.

8. Choi, B.D., Cai, M., Bigner, D.D., Mehta, A.I., Kuan, C.-T., and Sampson, J.H. (2011). Bispecific antibodies engage T cells for antitumor immunotherapy. Expet Opin. Biol. Ther. *11*, 843–853. https://doi.org/10.1517/14712598.2011.572874.

9. Firer, M.A., and Gellerman, G. (2012). Targeted drug delivery for cancer therapy: the other side of antibodies. J. Hematol. Oncol. *5*, 70. https://doi.org/10.1186/1756-8722-5-70.

10. Alley, S.C., Okeley, N.M., and Senter, P.D. (2010). Antibody–drug conjugates: targeted drug delivery for cancer. Curr. Opin. Chem. Biol. *14*, 529–537. https://doi.org/10.1016/j.cbpa.2010.06.170.

11. Maruani, A. (2018). Bispecifics and antibody–drug conjugates: A positive synergy. Drug Discov. Today Technol. *30*, 55–61. https://doi.org/10.1016/j.ddtec.2018.09.003.

12. Zhao, F., Wu, Y., Schaefer, K., Zhang, Y., Miao, K., Yao, Z., Ganjave, S.D., Kumru, K., Peters-Clarke, T.M., Inague, A., et al. (2025). Hijacking Extracellular Targeted Protein Degrader–Drug Conjugates for Enhanced Drug Delivery. J. Am. Chem. Soc. *147*, 39912–39925. https://doi.org/10.1021/jacs.5c15047.

13. Gu, Y., Wang, Z., and Wang, Y. (2024). Bispecific antibody drug conjugates: Making 1+1>2. Acta Pharm. Sin. B *14*, 1965–1986. https://doi.org/10.1016/j.apsb.2024.01.009.

14. De Nardis, C., Hendriks, L.J.A., Poirier, E., Arvinte, T., Gros, P., Bakker, A.B.H., and de Kruif, J. (2017). A new approach for generating bispecific antibodies based on a common light chain format and the stable architecture of human immunoglobulin G1. J. Biol. Chem. *292*, 14706–14717. https://doi.org/10.1074/jbc.M117.793497.

15. Klein, C., Schaefer, W., Regula, J.T., Dumontet, C., Brinkmann, U., Bacac, M., and Umaña, P. (2019). Engineering therapeutic bispecific antibodies using CrossMab technology. Methods *154*, 21–31. https://doi.org/10.1016/j.ymeth.2018.11.008.

16. Ridgway, J.B., Presta, L.G., and Carter, P. (1996). 'Knobs-into-holes' engineering of antibody $C_H3$ domains for heavy chain heterodimerization. Protein Eng. *9*, 617–621. https://doi.org/10.1093/protein/9.7.617.

17. Moldenhauer, G. (2011). Bispecific Antibodies from Hybrid Hybridoma. In Bispecific Antibodies (Springer Berlin Heidelberg), pp. 29–46. https://doi.org/10.1007/978-3-642-20910-9_2.

18. Zhang, X., Yang, Y., Fan, D., and Xiong, D. (2017). The development of bispecific antibodies and their applications in tumor immune escape. Exp. Hematol. Oncol. *6*, 12. https://doi.org/10.1186/s40164-017-0072-7.

19. Fan, G., Wang, Z., Hao, M., and Li, J. (2015). Bispecific antibodies and their applications. J. Hematol. Oncol. *8*, 130. https://doi.org/10.1186/s13045-015-0227-0.

20. Kontermann, R.E., and Brinkmann, U. (2015). Bispecific antibodies. Drug Discov. Today *20*, 838–847. https://doi.org/10.1016/j.drudis.2015.02.008.

21. Lee, J.H., Kim, J.W., Lee, H.E., Song, J.Y., Cho, A.H., Hwang, J.H., Heo, K., and Lee, S. (2024). A dual-targeting approach using a human bispecific antibody against the receptor-binding domain of the Middle East Respiratory Syndrome Coronavirus. Virus Res. *345*, 199383. https://doi.org/10.1016/j.virusres.2024.199383.

22. Mabry, R., Lewis, K.E., Moore, M., McKernan, P.A., Bukowski, T.R., Bontadelli, K., Brender, T., Okada, S., Lum, K., West, J., et al. (2010). Engineering of stable bispecific antibodies targeting IL-17A and IL-23. Protein Eng. Des. Sel. *23*, 115–127. https://doi.org/10.1093/protein/gzp073.

23. Karbyshev, M.S., Kalashnikova, I.V., Dubrovskaya, V.V., Baskakova, K.O., Kuzmichev, P.K., and Sandig, V. (2025). Trends and challenges in bispecific antibody production. J. Chromatogr. A *1744*, 465722. https://doi.org/10.1016/j.chroma.2025.465722.

24. Gordon, C.G., and Bertozzi, C.R. (2017). *In Vivo* Applications of Bioorthogonal Chemistries. In Chemoselective and Bioorthogonal Ligation Reactions (Wiley), pp. 417–457. https://doi.org/10.1002/9783527683451.ch14.

25. Fawcett, C., Watson, J., Richards, S., Doherty, A.E., Seki, H., Love, E.A., Coles, C.H., Coe, D.M., and Jamieson, C. (2025). Comparative Study of Click Handle Stability in Common Ligation Conditions. Bioconjug. Chem. *36*, 1054–1065. https://doi.org/10.1021/acs.bioconjchem.5c00095.

26. Brinkmann, U., and Kontermann, R.E. (2017). The making of bispecific antibodies. mAbs *9*, 182–212. https://doi.org/10.1080/19420862.2016.1268307.

27. Handula, M., Chen, K.-T., and Seimbille, Y. (2021). IEDDA: An Attractive Bioorthogonal Reaction for Biomedical Applications. Molecules *26*, 4640. https://doi.org/10.3390/molecules26154640.

28. Knall, A.-C., Hollauf, M., and Slugovc, C. (2014). Kinetic studies of inverse electron demand Diels–Alder reactions (iEDDA) of norbornenes and 3,6-dipyridin-2-yl-1,2,4,5-tetrazine. Tetrahedron Lett. *55*, 4763–4766. https://doi.org/10.1016/j.tetlet.2014.07.002.

29. Karver, M.R., Weissleder, R., and Hilderbrand, S.A. (2011). Synthesis and Evaluation of a Series of 1,2,4,5-Tetrazines for Bioorthogonal Conjugation. Bioconjug. Chem. *22*, 2263–2270. https://doi.org/10.1021/bc200295y.

30. Maruani, A., Szijj, P.A., Bahou, C., Nogueira, J.C.F., Caddick, S., Baker, J.R., and Chudasama, V. (2020). A Plug-and-Play Approach for the *De Novo* Generation of Dually Functionalized Bispecifics. Bioconjug. Chem. *31*, 520–529. https://doi.org/10.1021/acs.bioconjchem.0c00002.

31. Szijj, P.A., Gray, M.A., Ribi, M.K., Bahou, C., Nogueira, J.C.F., Bertozzi, C.R., and Chudasama, V. (2023). Chemical generation of checkpoint inhibitory T cell engagers for the treatment of cancer. Nat. Chem. *15*, 1636–1647. https://doi.org/10.1038/s41557-023-01280-4.

32. Lyu, Z., Kang, L., Buuh, Z.Y., Jiang, D., McGuth, J.C., Du, J., Wissler, H.L., Cai, W., and Wang, R.E. (2018). A Switchable Site-Specific Antibody Conjugate. ACS Chem. Biol. *13*, 958–964. https://doi.org/10.1021/acschembio.8b00107.

33. Schimek, C., Kubek, M., Scheich, D., Fink, M., Brocard, C., Striedner, G., Cserjan-Puschmann, M., and Hahn, R. (2021). Three-dimensional chromatography for purification and characterization of antibody fragments and related impurities from Escherichia coli crude extracts. J. Chromatogr. A *1638*, 461702. https://doi.org/10.1016/j.chroma.2020.461702.

34. Sivelle, C., Sierocki, R., Ferreira-Pinto, K., Simon, S., Maillere, B., and Nozach, H. (2018). Fab is the most efficient format to express functional antibodies by yeast surface display. mAbs *10*, 720–729. https://doi.org/10.1080/19420862.2018.1468952.

35. Junutula, J.R., Bhakta, S., Raab, H., Ervin, K.E., Eigenbrot, C., Vandlen, R., Scheller, R.H., and Lowman, H.B. (2008). Rapid identification of reactive cysteine residues for site-specific labeling of antibody-Fabs. J. Immunol. Methods *332*, 41–52. https://doi.org/10.1016/j.jim.2007.12.011.

36. Hutchins, B.M., Kazane, S.A., Staflin, K., Forsyth, J.S., Felding-Habermann, B., Schultz, P.G., and Smider, V.V. (2011). Site-Specific Coupling and Sterically Controlled Formation of Multimeric Antibody Fab Fragments with Unnatural Amino Acids. J. Mol. Biol. *406*, 595–603. https://doi.org/10.1016/j.jmb.2011.01.011.

37. Wozniak-Knopp, G., Stadlmayr, G., Perthold, J.W., Stadlbauer, K., Gotsmy, M., Becker, S., and Rüker, F. (2018). An antibody with Fab-constant domains exchanged for a pair of CH3 domains. PLoS One *13*, e0195442. https://doi.org/10.1371/journal.pone.0195442.

38. Maruani, A., Smith, M.E.B., Miranda, E., Chester, K.A., Chudasama, V., and Caddick, S. (2015). A plug-and-play approach to antibody-based therapeutics via a chemoselective dual click strategy. Nat. Commun. *6*, 6645. https://doi.org/10.1038/ncomms7645.

39. Bahou, C., and Chudasama, V. (2022). The use of bromopyridazinedione derivatives in chemical biology. Org. Biomol. Chem. *20*, 5879–5890. https://doi.org/10.1039/D2OB00310D.

40. Robinson, E., Nunes, J.P.M., Vassileva, V., Maruani, A., Nogueira, J.C.F., Smith, M.E.B., Pedley, R.B., Caddick, S., Baker, J.R., and Chudasama, V. (2017). Pyridazinediones deliver potent, stable, targeted and efficacious antibody–drug conjugates (ADCs) with a controlled loading of 4 drugs per antibody. RSC Adv. *7*, 9073–9077. https://doi.org/10.1039/C7RA00788D.

41. Chudasama, V., Smith, M.E.B., Schumacher, F.F., Papaioannou, D., Waksman, G., Baker, J.R., and Caddick, S. (2011). Bromopyridazinedione-mediated protein and peptide bioconjugation. Chem. Commun. *47*, 8781–8783. https://doi.org/10.1039/c1cc12807h.

42. Bahou, C., Richards, D.A., Maruani, A., Love, E.A., Javaid, F., Caddick, S., Baker, J.R., and Chudasama, V. (2018). Highly homogeneous antibody modification through optimisation of the synthesis and conjugation of functionalised dibromopyridazinediones. Org. Biomol. Chem. *16*, 1359–1366. https://doi.org/10.1039/C7OB03138F.

43. Wagh, A., Song, H., Zeng, M., Tao, L., and Das, T.K. (2018). Challenges and new frontiers in analytical characterization of antibody-drug conjugates. mAbs *10*, 222–243. https://doi.org/10.1080/19420862.2017.1412025.

44. Thoreau, F., Rochet, L.N.C., Baker, J.R., and Chudasama, V. (2023). Enabling the formation of native mAb, Fab′ and Fc-conjugates using a bis-disulfide bridging reagent to achieve tunable payload-to-antibody ratios (PARs). Chem. Sci. *14*, 3752–3762. https://doi.org/10.1039/D2SC06318B.

45. Thoreau, F., Szijj, P.A., Greene, M.K., Rochet, L.N.C., Thanasi, I.A., Blayney, J.K., Maruani, A., Baker, J.R., Scott, C.J., and Chudasama, V. (2023). Modular Chemical Construction of IgG-like Mono- and Bispecific Synthetic Antibodies (SynAbs). ACS Cent. Sci. *9*, 476–487. https://doi.org/10.1021/acscentsci.2c01437.

46. Pedregosa, F., Varoquaux, G., Gramfort, A., Michel, V., Thirion, B., Grisel, O., Blondel, M., Müller, A., Nothman, J., Louppe, G., et al. (2011). Scikit-learn: Machine Learning in Python. J. Mach. Learn. Res. *12*, 2825–2830.

47. Hunter, J.D. (2007). Matplotlib: A 2D Graphics Environment. Comput. Sci. Eng. *9*, 90–95. https://doi.org/10.1109/MCSE.2007.55.

## STAR★METHODS

### KEY RESOURCES TABLE

| REAGENT or RESOURCE | SOURCE | IDENTIFIER |
|---|---|---|
| Antibodies | | |
| Trastuzumab | MedChemExpress | Cat#HY-P9907; RRID:AB_2938985 |
| Rituximab | MedChemExpress | Cat#HY-P9913; RRID:AB_3694972 |
| Cetuximab | MedChemExpress | Cat#HY-P9905; RRID:AB_3694544 |
| Fab-specific anti-human IgG-HRP | Sigma-Aldrich | Cat#A0293; RRID:AB_257875 |
| Chemicals, peptides, and recombinant proteins | | |
| Immobilized pepsin | Thermo Scientific | Cat#20343 |
| Immobilized papain | Thermo Scientific | Cat#20341 |
| Endo-BCN-PEG2-amine | BroadPharm | Cat#BP-25106 |
| TCO-PEG3-amine | MedChemExpress | Cat#HY-141178 |
| Methyltetrazine-PEG4-amine | MedChemExpress | Cat#HY-14126 |
| $Br_2$PD-Tz-$N_3$ | Szijj et al.[31] | N/A |
| TAMRA-PEG4-DBCO | BroadPharm | Cat#BP-22456 |
| DBCO-PEG4-Val-Cit-PAB-$MMAE_t$ | BroadPharm | Cat#BP-25659 |
| Deposited data | | |
| Raw and analyzed data | This paper | Supplementary information available at DOI: https://doi.org/10.17632/xx6zczcxzm.1 |
| Critical commercial assays | | |
| Pierce BCA Protein Assay Kit | Thermo Scientific | Cat#23227 |
| Software and algorithms | | |
| Prism, v 8.0.1 | GraphPad | https://www.graphpad.com/ |
| Analyst TF, v 1.7.1 | AB Sciex Instruments | https://sciex.com/products/software/analyst-tf-software |
| PeakView, v 2.2 | AB Sciex Instruments | https://sciex.com/products/software/peakview-software |
| MestReNova, v 6.0.2–5475 | Mestrelab Research | https://mestrelab.com/download |
| Statistica, v 14.0.1.25 | TIBCO Software | https://docs.tibco.com/products/tibco-statistica-14-0-1 |
| scikit-learn | Pedregosa et al.[46] | https://scikit-learn.org/stable/ |
| matplotlib | JD Hunter[47] | https://matplotlib.org/ |
| Other | | |
| Superdex 200 Increase 10/300 GL | Cytiva | Cat#28990944 |
| NAb™ Protein A Plus Spin Columns | Thermo Scientific | Cat#89952 |

### METHOD DETAILS

#### BCA assay

The concentration of the $Fab_2$ external standards was measured using the Pierce BCA Protein Assay Kit (Cat. No. 23227). BSA solutions in PBS buffer were used as calibration standards (2000 μg/mL, 1500 μg/mL, 1000 μg/mL, 750 μg/mL, 500 μg/mL, 250 μg/mL, 125 μg/mL, 25 μg/mL, 0 μg/mL). The working reagent was prepared according to the user's guide, by mixing 50 parts of BCA reagent A with 1 part of BCA reagent B. 5 μL of each sample or standard were pipetted into the appropriate wells of a microplate (Greiner 96-well plate, Item No. 655101). 100 μL working reagent was added to each well, then mixed with a plate shaker for 30 s. After incubating the plate at 37°C for 30 min, absorbance was measured at 562 nm and was corrected by subtracting the average of negative controls. Each sample and standard were tested in triplicates. The measured absorbances of the standards were plotted against their concentration in μg/mL using Graphpad Prism. A linear model was fitted to the data points. This equation was used to determine the protein concentration of the unknown samples.

### Bradford assay

The concentration of the bispecific TAMRA conjugates was measured by a Bradford assay. Trastuzumab solutions in PBS buffer were used as calibration standards (2000 μg/mL, 1500 μg/mL, 1000 μg/mL, 750 μg/mL, 500 μg/mL, 250 μg/mL, 125 μg/mL, 25 μg/mL, 0 μg/mL). 5 μL of each sample or standard were pipetted into the appropriate wells of a microplate (Greiner 96-well plate, Item No. 655101). 250 μL Bradford reagent (a filtered solution of 5.9 mg Coomassie Blue G250, 50 mL MeOH and 11.8 mL 85% $H_3PO_4$ in 100 mL distilled water) was added to each well, then mixed with a plate shaker for 30 s. After incubating the plate at RT for 5 min, absorbance was measured at 595 nm and was corrected by subtracting the average of negative controls. Each sample and standard were tested in triplicates. The measured absorbances of the standards were plotted against their concentration in μg/mL using Graphpad Prism. A quadratic curve was fitted to the data points. This standard curve was used to determine the protein concentration of the unknown samples.

### Size-exclusion chromatography (SEC)

Purification by size-exclusion chromatography (SEC) was carried out on an ÄKTA go protein purification system (column: Superdex 200 increase, 10/300 GL), equilibrated in PBS pH 7.4. Flow rate during separation: 0.4 mL/min. Detection was by absorption at 280 nm.

### Hydrophobic interaction chromatography (HIC)

Hydrophobic interaction chromatography (HIC) was performed on an Agilent 1100 HPLC system (Agilent Technologies). Separations were carried out using a TSKgel HIC column (3.5 cm × 4.6 mm., 2.5 μm particle size). Protein samples were injected at a concentration of 1 mg/mL with an injection volume of 20 μL. Prior to separation, samples were equilibrated in Eluent A consisting of 1.5 M ammonium sulfate in 50 mM sodium phosphate buffer. Elution was performed using a linear gradient to Eluent B (50 mM sodium phosphate buffer) at a flow rate of 0.7 mL/min. The gradient profile was as follows: 100% Eluent A from 0 to 3 min, a linear transition from 100% A to 100% B between 3 and 15 min, followed by re-equilibration to 100% Eluent A from 15 to 18 min. UV detection was used for monitoring, and data acquisition and analysis were performed using the Agilent ChemStation software. Retention times of conjugated constructs were compared to that of native $F(ab')_2$ reference to assess relative changes in hydrophobicity.

### Protein LC-MS

The molecular weights of the Fab conjugates were identified using a Triple TOF 5600+ hybrid Quadrupole-TOF LC/MS/MS system (Sciex, Singapore, Woodlands) equipped with a DuoSpray IonSource coupled with a Shimadzu Prominence LC20 UFLC (Shimadzu, Japan) system consisting of binary pump, an autosampler, and a thermostated column compartment. Data acquisition and processing were performed using Analyst TF software version 1.7.1 (AB Sciex Instruments, CA, USA). Chromatographic separation was achieved on PLRP-S, 1000 Å, 8 μM, 150 mM × 2.1 mM column (Agilent, UK). The separation was achieved using mobile phase A (5% MeCN in 0.1% formic acid) and B (95% MeCN, 5% water 0.1% formic acid) using a gradient elution. The samples were diluted with ultrapure water, and the concentration set to 1 mg/mL. Flow rate was set to 0.5 mL/min. The column temperature was 60°C and the injection volume was 10 μL. $N_2$ was used as the nebulizer gas (GS1), heater gas (GS2), and curtain gas with the optimum values set at 40, 45 and 40 (arbitrary units), respectively. Data were acquired in positive ESI mode in the mass range of m/z = 500 to 5000, with 1 s accumulation time. The source temperature was 400°C and the spray voltage was set to 5000 V. Declustering potential value was set to 80 V. PeakView V.2.2 (version 2.2, Sciex, Redwood City, CA, USA) was used for deconvoluting the raw electrospray data to obtain the neutral molecular masses.

### SDS-PAGE gels

Non-reducing SDS-PAGE with 10% acrylamide gels were performed following standard lab procedures. A 5% stacking gel was used and a broad-range MW marker (4.6–315 kDa, ProSieve QuadColor Protein Marker, Lonza Bioscience) was co-run to estimate protein masses. Samples (5 μL at ~20 μM protein) were mixed with loading buffer (2 μL, composition for 6 × SDS: 1 g SDS, 3 mL glycerol, 6 mL 0.5 M Tris buffer pH 6.8, 2 mg Coomassie-blue R250 in 10 mL) and heated at 65°C for 5 min 7–10 μL of the samples was loaded into each well. The gels were run at 200 V for 60–90 min in 1 × SDS running buffer. Gels were stained using a Coomassie stain (0.12 g Coomassie-blue G-250, 0.10 g Coomassie-blue R-250, 500 mL MeOH, 400 mL distilled water, 100 mL acetic acid), after washing the gel was left at room temperature for 16 h in a water-ethanol mixture. Then the gels were imaged using HP Laserjet 1132 MFP scanner at 600 dpi. Images were saved under default brightness, contrast, and gamma settings. Fluorescent imaging (where applicable) was carried out before Coomassie Blue staining, using a ChemiDoc MP Imaging System (Bio-Rad).

### UV-Vis-spectroscopy

UV-Vis spectroscopy was used to determine the concentrations of protein constructs using a SpectraMax iD5 Multi-Mode Microplate Reader (Molecular Devices; San Jose, CA) operating at RT. Sample buffer was used as blank for baseline correction. Extinction

coefficients (Ɛ) for proteins and small molecules (at 280 nm) are listed below. The $Ɛ_{280}$ of the protein was added to that of the conjugated small molecules to calculate the total Ɛ of the construct at 280 nm ($\sum\varepsilon_{280}$). The concentration (c) of the construct was determined by the following equation:

$$c = \frac{A_{280}}{l \cdot \sum \varepsilon_{280}}$$

The extinction coefficient (Ɛ) values of proteins and small molecules at 280 nm: $Fab_{HER2}$ 68,590 $M^{-1}cm^{-1}$; $Fab_{CD20}$ 82,905 $M^{-1}cm^{-1}$; $Fab_{HER2}$×BCN 72,211 $M^{-1}cm^{-1}$; $Fab_{HER2}$×TCO 70,879 $M^{-1}cm^{-1}$; $Fab_{HER2}$×Tz 96,930 $M^{-1}cm^{-1}$; $Fab_{CD20}$×Tz-$N_3$ 109,658 $M^{-1}cm^{-1}$.

### HER2 ELISA

A 96-well plate was coated for 1 h at RT with HER2 (Sino Biological, 100 μL/well, 0.25 μg/mL, 3.5 nM in PBS). After washing (3 × 0.1% Tween 20 in PBS, followed by 3 × PBS), the wells were blocked for 1 h at RT with 1% BSA in PBS (150 μM, 200 μL/well). The wells were then washed and the following dilutions of $Fab_{HER2}$×$Fab_{CD20}$×TAMRA conjugates and $Fab_{HER2}$ were applied: 200 nM, 25 nM, 3.13 nM, 0.39 nM, 48.8 pM, 6.1 pM, prepared in PBS (100 μL/well). The assay was then incubated at RT for 1 h, washed and the detection antibody (Anti-Human IgG, Fab specific-HRP antibody, Sigma Aldrich, 1:5000 (ca. 10 nM) in 1% BSA in 0.1% Tween 20 in PBS) was added (100 μL/well). After 1 h at RT, the plates were washed and *o*-phenylenediamine hydrochloride (Sigma-Aldrich, 100 μL/well, 0.5 mg/mL, 2.8 mM in a phosphate-citrate buffer with sodium perborate) was added. Once a yellow-orange color was observed, the reaction was stopped by addition of HCl (4 M, 50 μL/well). Absorbance was immediately measured at 450 nm and was corrected by subtracting the average of negative controls. Each sample was tested in triplicate and errors are shown as the standard deviation of the mean. ELISA data was analyzed with Graphpad Prism.

### CD20 ELISA

A 96-well plate was coated for 1 h at RT with CD20 (Sino Biological, 100 μL/well, 0.2 μg/mL, 8 nM in PBS). After washing (3 × 0.1% Tween 20 in PBS, followed by 3 × PBS), the wells were blocked for 1 h at RT with 1% BSA in PBS (150 μM, 200 μL/well). The wells were then washed and the following dilutions of $Fab_{HER2}$×$Fab_{CD20}$×TAMRA conjugates and $Fab_{CD20}$ were applied: 4.8 μM, 0.8 μM, 133.3 nM, 22.2 nM, 3.70 nM, 0.62 nM, 0.10 nM prepared in PBS (100 μL/well). The assay was then incubated at RT for 1 h, washed and the detection antibody (Anti-Human IgG, Fab specific-HRP antibody, Sigma Aldrich, 1:5000 (ca. 10 nM) in 1% BSA in 0.1% Tween 20 in PBS) was added (100 μL/well). After 1 h at RT, the plates were washed and *o*-phenylenediamine hydrochloride (Sigma-Aldrich, 100 μL/well, 0.5 mg/mL, 2.8 mM in a phosphate-citrate buffer with sodium perborate) was added. Once a yellow-orange color was observed, the reaction was stopped by addition of HCl (4 M, 50 μL/well). Absorbance was immediately measured at 450 nm and was corrected by subtracting the average of negative controls. Each sample was tested in triplicate and errors are shown as the standard deviation of the mean. ELISA data was analyzed with Graphpad Prism.

### Production of $Fab_{HER2}$

300 μL (19.97 mg/mL) trastuzumab mAb sample was buffer exchanged into pepsin digest buffer (20 mM NaOAc, pH 3.1). Immobilized pepsin (732 μL) was washed 3 times with pepsin digest buffer, then the mAb solution was added. The mixture was incubated for 5 h at 37°C under constant agitation (1100 rpm). The agarose resin was separated from the digest by using a filter column, then washed twice with papain digest buffer (50 mM $Na_2HPO_4$, 150 mM NaCl, 1 mM EDTA, pH 6.8). The digest and the washes were combined, concentrated, then the buffer was completely exchanged for the papain digest buffer.

Immobilized papain (1220 μL, 250 μg/mL) was activated by 10 mM DTT (in papain digest buffer) for an hour at 37°C under constant agitation (1000 rpm). The resin was washed 10 times with DTT-free papain digest buffer, then the $F(ab')_2$ solution was added. The mixture was incubated for 16 h at 37°C under constant agitation (1100 rpm). The agarose resin was separated from the digest by using a filter column, then washed twice with papain digest buffer. The digest and the washes were combined, and the buffer was exchanged for PBS buffer (137 mM NaCl, 3.7 mM KCl, 10 mM $Na_2HPO_4$, 1.8 mM $KH_2PO_4$, pH 7.4), yielding 150 μL 98.65 μM Fab solution.

### Production of $Fab_{CD20}$

100 μL (9.97 mg/mL) rituximab mAb sample was buffer exchanged into papain digest buffer (50 mM $Na_2HPO_4$, 150 mM NaCl, 1 mM EDTA, pH 6.8). Immobilized papain (100 μL, 250 μg/mL) was activated by 10 mM DTT (in papain digest buffer) for an hour at 37°C under constant agitation (1000 rpm). The resin was washed 10 times with DTT-free papain digest buffer, then the mAb solution was added. The mixture was incubated for 16 h at 37°C under constant agitation (1100 rpm). The agarose resin was separated from the digest by using a filter column, then washed twice with papain digest buffer. The digest and the washes were combined, and the buffer was exchanged completely for PBS (pH 7.4). Then, the sample was applied to a NAb protein A Plus column (Thermo Scientific) and incubated at 25°C under constant agitation (300 rpm) for 30 min. The Fab fraction was eluted according to

manufacturers' protocol, the column washed three times with PBS (pH 7.4) and the Fc fraction eluted three times with 100 mM glycine, pH 2.5, which was neutralized with 40 μL 1 M Tris, pH 8.8 solution. The Fab fraction was combined with the washes then buffer exchanged into PBS (pH 7.4), yielding 100 μL 44.87 μM Fab solution.

### Production of $Fab_{EGFR}$

500 μL (5 mg/mL) cetuximab mAb sample was buffer exchanged into digest buffer (20 mM $Na_2HPO_4$, 10 mM EDTA, 80 mM cysteine, pH 7). Immobilized papain (650 μL, 250 μg/mL) was washed 3 times with digest buffer, then the mAb solution was added. The mixture was incubated for 4 h at 37°C under constant agitation (1100 rpm). The agarose resin was separated from the digest by using a filter column, then washed twice with papain digest buffer. The digest and the washes were combined, and the buffer was exchanged completely for PBS (pH 7.4). Then, the sample was applied to a NAb protein A Plus column (Thermo Scientific) and incubated at 25°C under constant agitation (300 rpm) for 30 min. The Fab fraction was eluted according to manufacturers' protocol, the column washed three times with PBS (pH 7.4) and the Fc fraction eluted three times with 100 mM glycine, pH 2.5, which was neutralized with 40 μL 1 M Tris, pH 8.8 solution. The Fab fraction was combined with the washes then buffer exchanged into PBS (pH 7.4), yielding 116 μL 125.5 μM Fab solution.

### Production of $F(ab')_{2,HER2}$

300 μL (19.97 mg/mL) trastuzumab mAb sample was buffer exchanged into pepsin digest buffer (20 mM NaOAc, pH 3.1). Immobilized pepsin (732 μL) was washed 3 times with pepsin digest buffer, then the mAb solution was added. The mixture was incubated for 5 h at 37°C under constant agitation (1100 rpm). The agarose resin was separated from the digest by using a filter column, then washed twice with PBS (7.4). The digest and the washes were combined, concentrated, then the buffer was completely exchanged for PBS (7.4). The mixture was purified by SEC as described above.

### Chemical modification of fab

Fab solution was diluted to 20 μM with 1.1 mM solution of TCEP HCl in BBS (pH 8.8) (50 eq.), then incubated at 37°C for 90 min under constant agitation (500 rpm). The reaction mixture was then buffer exchanged into TCEP-free PBS (pH 7.4) and diluted to its original volume. 5 equivalents of the rebridging agent (**$Br_2$PD-BCN**, **$Br_2$PD-TCO**, **$Br_2$PD-Tz**) was added (5 mM solution in DMSO) to this solution, then the mixture was incubated at 37°C for another 90 min under constant agitation (500 rpm). The modified Fabs thus prepared were purified by membrane filtration (Vivaspin 10 kDa), followed by filtration through Zeba Spin Desalting Column (7 K MWCO).

### Preparation of $Fab_{HER2}$×$Fab_{HER2}$ MS standards

To a solution of $Fab_{HER2}$×Tz (40 μL, 200 μM, in pH 7.4 PBS), 1 equivalent of $Fab_{HER2}$×BCN or $Fab_{HER2}$×TCO (40 μL, 200 μM, in pH 7.4 PBS) was added and the mixture was incubated at 37°C overnight under constant agitation (300 rpm). The mixture was purified by SEC. The concentration of the purified standards was measured using BCA assay.

### Experimental procedure of the DOE analysis

Fab×BCN, Fab×TCO and Fab×Tz was buffer exchanged into PBS (pH 5, 7 or 9) then diluted to the appropriate concentration (200 μM, 120 μM or 40 μM). For each sample 7.5 μL Fab×BCN or Fab×TCO and 7.5 μL Fab×Tz solution were mixed in equimolar ratio then incubated at 4, 20.5 or 37°C. After the designated reaction time, the samples were quenched with 3,6-di(4-pyridyl)-1,2,4,5-tetrazine (0.3 μL, 5 mM, in DMSO).

### DoEs

To investigate the influence of reaction conditions (temperature, pH, reaction time, and starting concentration) on conjugation efficiency, a $2^4$ full factorial experimental design was employed with five center points (21 experiments altogether). Factorial analysis of variance (ANOVA) was applied in the STATISTICA software (version 14.0.1.25, TIBCO Software Inc.) to establish statistical significance of the four main factors, as well as their pairwise interactions. Response surface plots were generated with the scikit-learn python package[46] and matplotlib.[47]

### Investigating the effect of molar excess

Fab×BCN, Fab×TCO and Fab×Tz was buffer exchanged into pH 5 PBS then diluted to 300 μM. Samples were prepared in duplicates. Reactions were incubated at 4°C for 16 h, then quenched with 3,6-di(4-pyridyl)-1,2,4,5-tetrazine (0.3 μL, 5 mM, in DMSO) and submitted to LC-MS analysis.

### Preparation of $Fab_{HER2}$×$Fab_{CD20}$×TAMRA

$Fab_{HER2}$×BCN, $Fab_{HER2}$×TCO and $Fab_{CD20}$×Tz-$N_3$ was buffer exchanged into pH 5 PBS. To a solution of $Fab_{CD20}$×Tz-$N_3$ (19 μL, 148.64 μM, 1 eq.), TAMRA-PEG4-DBCO was added (dissolved in DMSO, 0.28 μL, 20 mM, 2 eq.) and the mixture incubated at 37°C for 1 h under constant agitation (300 rpm). After this time, 1 equivalent of $Fab_{HER2}$×BCN (12.51 μL, 225.73 μM) or $Fab_{HER2}$×TCO (10.55 μL, 267.78 μM) was added and the mixture was incubated at 4°C overnight. The mixture was purified by SEC, resulting in the representative isolated yield of 61% for BCN-Tz and 68% for TCO-Tz constructs.

### Preparation of $Fab_{HER2}$×$Fab_{EGFR}$×MMAE

$Fab_{HER2}$×BCN, $Fab_{HER2}$×TCO and $Fab_{EGFR}$×Tz-$N_3$ was buffer exchanged into pH 5 PBS. To a solution of $Fab_{EGFR}$×Tz-$N_3$ (8.35 μL, 311.5 μM, 1 eq.), MMAE-vcPAB-PEG4-DBCO was added (dissolved in DMSO, 1.3 μL, 20 mM, 10 eq.) and the mixture incubated at 37°C for 1 h under constant agitation (300 rpm). After this time, 1 equivalent of $Fab_{HER2}$×BCN (19.71 μL, 132 μM) or $Fab_{HER2}$×TCO (16.77 μL, 160 μM) was added and the mixture was incubated at 4°C overnight. The mixture was purified by SEC, resulting in the representative isolated yield of 57% for BCN-Tz and 65% for TCO-Tz constructs.

### Chemical synthesis

All commercially available reagents were used as received. The reactions were followed by HPLC–MS chromatography with a Shimadzu LCMS-2020 device using a Reprospher 100 C18 (5 μm; 100 × 3 mm) column and positive-negative double ion source (DUIS) with a quadrupole MS analyzer in a range of 50–1000 m/z. High resolution mass spectra were recorded on a Waters Q-TOF Premier mass spectrometer in positive ESI ionization mode. $^{1}H$ and $^{13}C$ NMR spectra were recorded in $CDCl_3$ or DMSO-d6 solution at room temperature, on a Varian Unity Inova 500 spectrometer (500 and 125 MHz for $^{1}H$ and $^{13}C$/APT NMR spectra, respectively), and on a Varian Unity Inova 300 spectrometer (300, 75 MHz and 282 MHz for $^{1}H$, APT NMR spectra, respectively), with the deuterium signal of the solvent as the lock. Chemical shifts (δ) and coupling constants (J) are given in ppm and Hz, respectively. The antibody solutions were centrifuged with Eppendorf Centrifuge 5810 R.

#### *Di-tert-butyl 1-methylhydrazine-1,2-dicarboxylate ($Br_2$PD-1)*

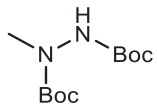


To a solution of methyl hydrazine (1 g, 21.7 mmol) in propan-2-ol (16 mL), was added dropwise over 30 min a solution of di-*tert*-butyl dicarbonate (11.4 g, 52.1 mmol, dissolved in DCM (12 mL)). The reaction was then stirred at room temperature for 16 h. After this time, the solvents were removed *in vacuo* and the crude residue purified by flash column chromatography (0%–20% *n*-hexane/EtOAc) to yield **$Br_2$PD-1** (4.82 g, 19.7 mmol, 90%) as a white solid. $^{1}H$ NMR (500 MHz, $CDCl_3$, rotamers) δ 6.41-6.14 (m, 1H), 3.12 (s, 3H), 1.49-1.48 (m, 18H) ppm.

#### *Di-tert-butyl 1-(3-(tert-butoxy)-3-oxopropyl)-2-methylhydrazine-1,2-dicarboxylate ($Br_2$PD-2)*

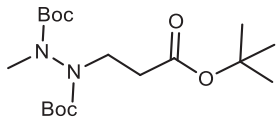


To a solution of **$Br_2$PD-1** (4.00 g, 16.3 mmol) in *tert*-butanol (62.4 g) was added 10% aq. NaOH (0.64 mL) and the reaction mixture stirred at room temperature for 5 min. After this time, *tert*-butyl acrylate (7.04 mL, 48.5 mmol) was added to the solution, and the reaction mixture was heated at 60°C overnight. Following this, the solvent was removed *in vacuo,* and the crude residue was dissolved in EtOAc (30 mL) and washed with water (3 × 20 mL). The organic layer was then dried ($MgSO_4$), filtered and the solvent removed *in vacuo*. Purification of the crude residue by flash column chromatography (0%–50% *n*-hexane/EtOAc) yielded **$Br_2$PD-2** (4.19 g, 11.2 mmol, 69%) as a clear oil. $^{1}H$ NMR (500 MHz, $CDCl_3$, rotamers) δ 3.86-3.55 (m, 2H), 3.10-3.00 (m, 3H), 2.53 (t, J = 7.5 Hz, 2H), 1.52-1.43 (m, 27H) ppm.

#### *3-(4,5-Dibromo-2-methyl-3,6-dioxo-3,6-dihydropyridazin-1(2H)-yl)propanoic acid ($Br_2$PD-3)*

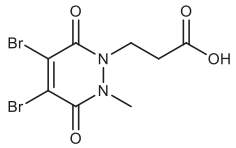

Dibromomaleic acid (3.5 g; 12.78 mmol) was dissolved in cc. AcOH (35 mL) and heated under reflux for 30 min. To this solution was added **$Br_2$PD-2** (4.17 g; 11.15 mmol) dissolved in cc. AcOH (15 mL) and the reaction heated under reflux for a further 4 h. The solvent was removed *in vacuo* and the crude residue purified by flash column chromatography (0–70% *n*-hexane/EtOAc) to yield **$Br_2$PD-3** (2.95 g, 8.25 mmol, 74%) as a yellow powder. $^1$H NMR (500 MHz, DMSO-d6) δ 12.46 (br s, 1H), 4.28 (t, J = 7.5 Hz, 2H), 3.57 (s, 3H), 2.63 (t, J = 7.5 Hz, 2H) ppm.

***2,5-Dioxopyrrolidin-1-yl 3-(4,5-dibromo-2-methyl-3,6-dioxo-3,6-dihydropyridazin-1(2H)-yl)propanoate ($Br_2$PD-4)***

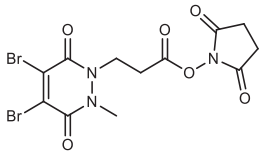

To a solution of **$Br_2$PD-3** (2.00 g; 5.62 mmol) in dry THF (100 mL) at 0°C was added DCC (1.33 g; 6.4 mmol). The solution was stirred at 0°C for 30 min. Following this, was added NHS (0.8 g, 6.9 mmol) and the reaction stirred at room temperature for a further 16 h. The solvent was removed *in vacuo* and the crude residue purified by flash column chromatography (0–100% *n*-hexane/EtOAc) to yield pyridazinedione **$Br_2$PD-4** (1.55 g, 3.43 mmol, 61%) as a white powder. $^1$H NMR (500 MHz, DMSO-d6) δ 4.41 (t, J = 7.5 Hz, 2H), 3.59 (s, 3H), 3.18 (t, J = 7.5 Hz, 2H), 2.82 (s, 4H) ppm.

***((1R,8S,9s)-Bicyclo[6.1.0]non-4-yn-9-yl)methyl (2-(2-(2-(3-(4,5-dibromo-2-methyl-3,6-dioxo-3,6-dihydropyridazin-1(2H)-yl)propanamido)ethoxy)ethoxy)ethyl) carbamate ($Br_2$PD-BCN)***

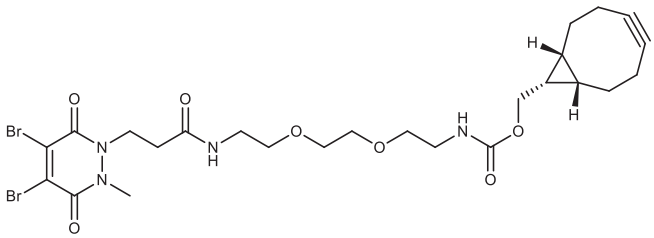

To a solution of BCN-PEG2-amine (10 mg, 30.8 μmol) in acetonitrile (5 mL), 15.36 mg (33.9 μmol, 1.1 eq.) **$Br_2$PD-4** was added. The solution was stirred at room temperature for 90 min. The solvent was removed *in vacuo* and the crude residue purified by preparative HPLC chromatography (0–100% (99.9% water, 0.1% HCOOH)/(99.9% acetonitrile, 0.1% HCOOH)) to yield **$Br_2$PD-BCN** as a yellow solid (5.4 mg, 8.2 μmol, 34%). $^1$H NMR (500 MHz, $CDCl_3$) δ 7.72 (br s, 0.1 H), 6.48 (br s, 0.5 H), 5.70 (br s, 0.1 H), 5.24 (br s, 0.5 H), 4.43 (t, J = 7 Hz, 2H), 4.15 (d, J = 7.4 Hz, 2H), 3.72 (s, 3H), 3.64-3.56 (m, 6H), 3.53 (t, J = 4.9 Hz, 2H), 3.44 (dd, $J_1$ = 10.2 Hz, $J_2$ = 5.2 Hz, 2H), 3.37 (m, 2H) 2.63 (t, J = 7 Hz, 2H), 2.34-2.17 (m, 6H), 1.64-1.53 (m, 2H), 1.40-1.29 (m, 1H), 1.00-0.90 (m, 2H) ppm. HRMS (ESI) calculated for $C_{25}H_{35}Br_2N_4O_7$ $[M^{79}Br^{81}Br+H]^+$ 663.0847, observed 663.0827.

***E-Cyclooct-4-en-1-yl (15-(4,5-dibromo-2-methyl-3,6-dioxo-3,6-dihydropyridazin-1(2H)-yl)-13-oxo-3,6,9-trioxa-12-azapentadecyl) carbamate ($Br_2$PD-TCO)***

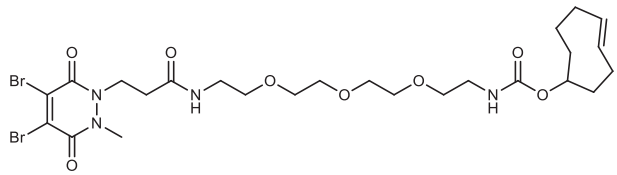

To a solution of TCO-PEG3-amine (10 mg, 29.0 μmol) in acetonitrile (5 mL), 14.45 mg (31.9 μmol, 1.1 eq.) **$Br_2$PD-4** was added. The solution was stirred at room temperature for 90 min. The solvent was removed *in vacuo* and the crude residue purified by preparative HPLC chromatography (0–100% (99.9% water, 0.1% HCOOH)/(99.9% acetonitrile, 0.1% HCOOH)) to yield **$Br_2$PD-TCO** as a yellow solid (10.9 mg, 15.7 μmol, 54%). $^1$H NMR (500 MHz, $CDCl_3$) δ 6.72 (br s, 1H), 5.63–5.47 (m, 2H), 5.29 (br s, 1H), 4.46 (t, *J* = 6.9 Hz, 2H), 4.38–4.32 (m, 1H), 3.75 (s, 3H), 3.63 (d, J = 5.4 Hz, 8H), 3.59–3.52 (m, 4H), 3.44 (q, *J* = 5 Hz, 2H), 3.36 (m, 2H), 2.63 (t, *J* = 6.9 Hz, 2H), 2.40–2.32 (m, 3H), 2.05–1.89 (m, 4H), 1.78–1.68 (m, 2H), 1.60–1.50 (m, 1H) ppm. HRMS (ESI) calculated for $C_{25}H_{38}Br_2N_4O_8$ $[M^{79}Br^{81}Br+H]^+$ 683.1109, observed 683.1137.

***3-(4,5-Dibromo-2-methyl-3,6-dioxo-3,6-dihydropyridazin-1(2H)-yl)-N-(2-(2-(2-(2-(4-(6-methyl-1,2,4,5-tetrazin-3-yl)phenoxy)ethoxy)ethoxy)ethoxy)ethyl) propanamide ($Br_2$PD-Tz)***

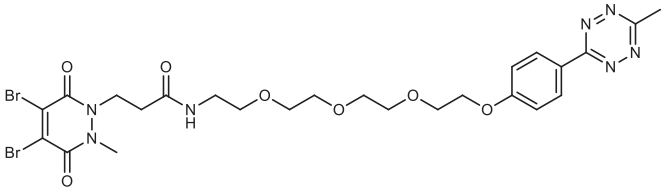

To a solution of methyl-tetrazine-PEG4-amine HCl (10 mg, 25.0 μmol) and 3.48 μL TEA (2.53 mg, 1 eq.) in acetonitrile (5 mL), 12.46 mg (27.5 μmol, 1.1 eq.) **$Br_2$PD-4** was added. The solution was stirred at room temperature for 90 min. The solvent was removed *in vacuo* and the crude residue purified by preparative HPLC chromatography (0–100% (99.9% water, 0.1% HCOOH)/(99.9% acetonitrile, 0.1% HCOOH)) to yield **$Br_2$PD-Tz** as a purple solid (2.7 mg, 3.76 μmol, 15%). $^1$H NMR (500 MHz, $CDCl_3$) δ 8.55 (d, J = 8.85 Hz, 2H), 7.11 (d, J = 8.85 Hz, 2H), 6.51 (br s, 0.8H), 4.43 (t, J = 6.9 Hz, 2H), 4.27 (t, J = 6.9 Hz, 2H), 3.93 (t, J = 6.9 Hz, 2H), 3.78 (m, 2H), 3.73-3.70 (m, 5H), 3.68-3.62 (m, 4H), 3.55 (t, J = 5 Hz, 2H), 3.44 (dd, $J_1$ = 10.2 Hz, $J_2$ = 5 Hz, 2H), 3.08 (s, 3H), 2.62 (t, J = 6.8 Hz, 2H) ppm. HRMS (ESI) calculated for $C_{25}H_{31}Br_2N_7O_7$ $[M^{79}Br^{81}Br+H]^+$ 702.0704, observed 702.0733.

***tert-Butyl (4-cyanobenzyl)carbamate ($Br_2$PD-5)***

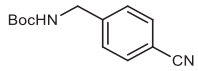

To a stirring solution of NaOH (3.6 g, 89.1 mmol) and di-*tert*-butyl dicarbonate (7.1 g, 32.6 mmol) in $H_2O$ (30 mL) was added, at room temperature, a pre-dissolved solution of 4-(aminomethyl)benzonitrile (5.0 g, 29.7 mmol) in $H_2O$ (30 mL). The mixture was stirred for 16 h, after which time a white precipitate had formed. The mixture was filtered, the solid washed with H2O (100 mL), and the resulting solid dried under vacuum to yield compound **$Br_2$PD-5** as a white solid (6.1 g, 26.2 mmol, 88%). $^1$H NMR (400 MHz, CDCl3) δ 7.62 (d, *J* = 8.3, 2H), 7.38 (d, *J* = 8.3, 2H), 4.96 (br. s, 1H), 4.37 (d, *J* = 5.9 Hz, 2H), 1.46 (s, 9H).

***tert-Butyl (4-(6-methyl-1,2,4,5-tetrazin-3-yl)benzyl)carbamate ($Br_2$PD-6)***

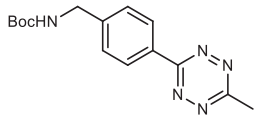

The following procedure was adapted from work by Lang et al.9 To a stirring suspension of *tert*-butyl carbamate **$Br_2$PD-5** (3.0 g, 12.9 mmol), acetonitrile (6.72 mL, 12.9 mmol), and Zn(OTf)2 (2.34 g, 6.46 mmol) in 1,4-dioxane (6 mL) was added, at room temperature, hydrazine hydrate (80% w/w, 39.5 mL, 646 mmol). The reaction was heated to 65°C and stirred for 72 h. After this time, the reaction was cooled to room temperature and diluted with EtOAc (50 mL). The mixture was washed with 1 M HCl (50 mL), and the aqueous phase extracted with EtOAc (2 × 30 mL). The organic phase was dried ($MgSO_4$), filtered and solvent was then removed *in vacuo*. The resulting crude residue was dissolved in a mixture of DCM and acetic acid (1:1, 200 mL), and to this was added $NaNO_2$ (17.8 g, 258 mmol) slowly over a period of 15 min, during which time the reaction turned bright red. The reaction was then diluted with DCM (200 mL), washed with sodium bicarbonate (sat. aq., 200 mL) and the aqueous phase extracted with DCM (2 × 100 mL). The organic phases were combined and then dried ($MgSO_4$), filtered and the solvent was then removed *in vacuo*. The resulting residue was purified by flash column chromatography (20% EtOAc/petrol) to yield tetrazine **$Br_2$PD-6** as a pink solid (1.07 g, 3.55 mmol, 28%). $^1$H NMR (400 MHz, CDCl3) δ 8.55 (d, *J* = 8.4 Hz, 2H), 7.50 (d, *J* = 8.3 Hz, 2H), 4.97 (br. s, 1H), 4.44 (d, *J* = 5.8 Hz, 2H), 3.09 (s, 3H), 1.48 (s, 9H).

***5-((4-(6-Methyl-1,2,4,5-tetrazin-3-yl)benzyl)amino)-5-oxopentanoic acid ($Br_2$PD-7)***

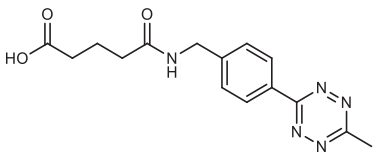

*Tert*-butyl (4-(6-methyl-1,2,4,5-tetrazin-3-yl)benzyl)carbamate **$Br_2$PD-6** (800 mg, 2.65 mmol) was dissolved in a mixture of TFA and DCM (1:4, 20 mL) and the solution was stirred at room temperature for 2 h. The solvent was then removed *in vacuo* and the mixture re-dissolved in THF (50 mL). To this solution was added glutaric anhydride (605 mg, 5.31 mmol) and the mixture stirred at 55°C for 16 h. The solvent was removed *in vacuo* and the mixture re-dissolved in sat. aq. $K_2CO_3$ solution (100 mL). The mixture was then acidified with 15% HCl aq. solution until the mixture stopped producing $CO_2$(g) on acid. The mixture was then extracted with EtOAc (3 × 50 mL), and the combined organic phases washed with $H_2O$ (4 × 30 mL) and brine (30 mL), and then dried ($MgSO_4$). Any precipitate formed during extraction was re-dissolved in sat. aq. $K_2CO_3$ solution (30 mL) and the work-up was repeated on this solution and the dried organic phases were combined, filtered and the solvent removed *in vacuo* to yield compound **$Br_2$PD-7** as a purple powder (691 mg, 2.2 mmol, 83%) without further purification. $^1$H NMR (400 MHz, CDCl3) δ 8.41 (d, *J* = 8.4, 2H), 7.51 (d, *J* = 8.5 Hz, 2H), 4.38 (d, *J* = 6.0 Hz, 2H), 4.27 (q, *J* = 7.4 Hz, 4H), 2.98 (s, 3H), 1.76 (quint., *J* = 7.4 Hz, 2H).

***$N^1$-(3-(2-(2-(2-azidoethoxy)ethoxy)ethoxy)ethyl)-$N^5$-(4-(6-methyl-1,2,4,5-tetrazin-3-yl) benzyl)glutaramide ($Br_2$PD-8)***

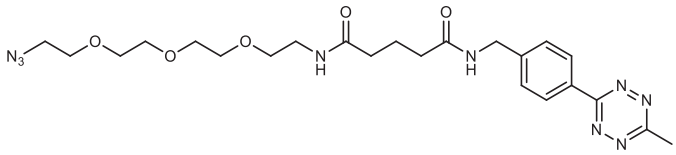

To a solution of 5-((4-(6-methyl-1,2,4,5-tetrazin-3-yl)benzyl)amino)-5-oxopentanoic acid **$Br_2$PD-7** (200 mg, 0.63 mmol) in DCM (5 mL) was added, at room temperature, HATU (240 mg, 0.63 mmol), and $NEt_3$ (87.8 μL, 0.63 mmol), and the reaction stirred for 5 min. Subsequently, to this solution was added, at room temperature, a solution of 2-(2-(2-(2-azidoethoxy)ethoxy)ethoxy)ethan-1-amine (387.5 μL, 1.96 mmol) in DCM (5 mL), and the resulting solution was stirred at room temperature for 16 h. The reaction was then diluted with EtOAc (25 mL) and H2O (25 mL) and the phases separated. The aqueous phase was extracted with EtOAc (3 × 25 mL) and the combined organic phases were washed with H2O (3 × 25 mL), brine (20 mL), dried (MgSO4), filtered and the solvent removed *in vacuo*. The crude residue was purified by flash column chromatography (0–10% MeOH in DCM) to afford **$Br_2$PD-8** (209.5 mg, 0.51 mmol, 64%) as a purple solid. $^1$H NMR (400 MHz, CDCl3) δ 8.55 (d, *J* = 8.4 Hz, 2H), 7.51 (d, *J* = 8.5 Hz, 2H), 6.61 (br. s, 1H), 6.16 (br. s, 1H), 4.55 (d, *J* = 6.0 Hz, 2H), 3.68–3.59 (m, 10 H), 3.56–3.52 (m, 2H), 3.45–3.36 (m, 4H), 3.09 (s, 3H), 2.35 (t, *J* = 7.1 Hz, 2H), 2.26 (t, *J* = 6.9 Hz, 2H), 2.01 (quint., *J* = 6.9 Hz, 2 H).

***Di*-tert-*butyl 1-(prop-2-yn-1-yl)hydrazine-1,2-dicarboxylate ($Br_2$PD-9)***

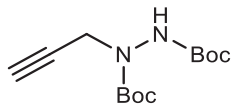

To a solution of di-*tert*-butyl hydrazine-1,2-dicarboxylate (3.00 g, 12.9 mmol) in a mixture of toluene (15 mL) and 5% aq. NaOH (15 mL) were added tetra-*n*-butylammonium bromide (104 mg, 0.32 mmol) and propargyl bromide (5.76 g, 38.7 mmol). The reaction mixture was stirred at 20°C for 16 h. After this time, $H_2O$ (20 mL) was added, and the mixture was extracted with EtOAc (3 × 30 mL). The combined organic layers were washed with brine (30 mL), dried ($MgSO_4$), filtered and the solvent removed *in vacuo*. Purification by flash column chromatography (20% EtOAc/petrol) yielded **$Br_2$PD-9** (2.04 g, 7.56 mmol, 59%) as a white solid. $^1$H NMR (400 MHz, CDCl3, rotamers) δ 6.48 (br. s, 0.7H), 6.17 (br. s, 0.2H), 4.27 (s, 2H), 2.24 (t, *J* = 2.4 Hz, 1H), 1.47 (s, 18H).

***Di*-tert-*butyl 1-(3-(tert-butoxy)-3-oxopropyl)-2-(prop-2-yn-1-yl)hydrazine-1,2-dicarboxylate ($Br_2$PD-10)***

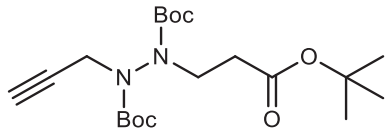

To a solution of di-*tert*-butyl 1-(prop-2-yn-1-yl)hydrazine-1,2-dicarboxylate **$Br_2$PD-9** (1.5 g, 5.55 mmol) in *tert*-BuOH (10 mL) and 5% NaOH solution (0.5 mL) was added *tert*-butyl acrylate (3.22 mL, 22.2 mmol) and the reaction mixture was heated at 60°C for 24 h. Following this, the solvent was removed *in vacuo* and the crude residue was dissolved in EtOAc (75 mL) and washed with $H_2O$ (3 × 25 mL). The organic layer was then dried ($MgSO_4$), filtered and the solvent removed *in vacuo* to afford **$Br_2$PD-10** (1.84 g, 4.6 mmol, 83%) as a clear oil. $^1$H NMR (400 MHz, CDCl3, rotamers) δ 4.69–3.58 (m, 2H), 3.85–3.65 (m, 2H), 2.69–2.60 (m, 2H), 2.27 (t, *J* = 2.5 Hz, 1H), 1.60–1.38 (m, 27H).

### 3-(4,5-Dibromo-3,6-dioxo-2-(prop-2-yn-1-yl)-3,6-dihydropyridazin-1(2H)-yl)propanoic acid ($Br_2$PD-11)

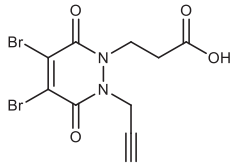

Dibromomaleic anhydride (1.13 g, 4.14 mmol) was dissolved in AcOH (30 mL) and heated under reflux for 30 min. To this solution was added di-*tert*-butyl 1-(3-(*tert*-butoxy)-3-oxopropyl)-2-(prop-2-yn-1-yl)hydrazine-1,2-dicarboxylate **$Br_2$PD-10** (1.5 g, 3.76 mmol) and the reaction heated under reflux for a further 4 h. The solvent was removed *in vacuo* by co-evaporation with toluene and the crude residue was purified by flash column chromatography (25–100% (99% EtOAc, 1% AcOH)/petrol) to yield **$Br_2$PD-11** (926 mg, 2.44 mmol, 65%) as a yellow powder. $^1$H NMR (400 MHz, DMSO-d6) δ 12.48 (br. s, 1 H), 4.91 (d, *J* = 2.4 Hz, 2H), 4.27 (t, *J* = 7.4 Hz, 2H), 3.53 (t, *J* = 2.4 Hz, 1H), 2.66 (t, *J* = 7.4 Hz, 2H).

### 3-(4,5-Dibromo-2-((1-(1-(4-(6-methyl-1,2,4,5-tetrazin-3-yl)phenyl)-3,7-dioxo-11,14,17-trioxa-2,8-diazanonadecan-19-yl)-1H-1,2,3-triazol-4-yl)methyl)-3,6-dioxo-3,6-dihydropyridazin-1(2H)-yl)propanoic acid ($Br_2$PD-12)

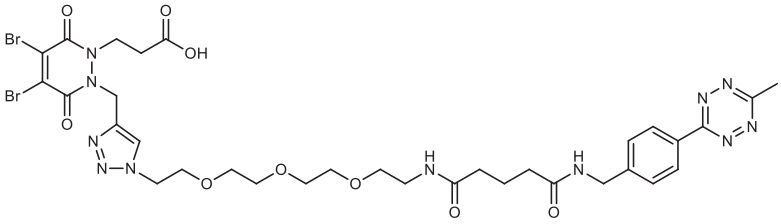

To a solution of *N*1-(2-(2-(2-(2-azidoethoxy)ethoxy)ethoxy)ethyl)-*N*5-(4-(6-methyl-1,2,4,5-tetrazin-3-yl)benzyl)glutaramide **$Br_2$PD-8** (50.0 mg, 97.0 μmol) and 3-(4,5-dibromo-3,6-dioxo-2-(prop-2-yn-1-yl)-3,6-dihydropyridazin-1(2*H*)-yl)propanoic acid **$Br_2$PD-11** (44.3 mg, 116.6 μmol) in THF (10 mL) at 21°C was added DIPEA (16.8 μL, 97.0 μmol) and CuI (9.4 mg, 48.5 μmol) and the mixture stirred at 21°C for 5 h. The mixture was then filtered, and the solvent removed *in vacuo*. The mixture was dissolved in $H_2O$ (10 mL) and basified with sat. aq. NaHCO3 (10 mL), and then washed with DCM (3 × 10 mL). The organic phase was discarded, and DCM (10 mL) was added to the aqueous phase. The aqueous phase was then acidified with 4 M HCl until the evolution of $CO_2$(g) stopped and the purple product mostly moved to the organic phase. The aqueous phase was then extracted with further DCM (3 × 10 mL). The combined organic phases were washed with brine, dried ($MgSO_4$), filtered and the solvent removed *in vacuo*. The crude residue was purified by flash column chromatography (0–20% (99% MeOH, 1% AcOH)/DCM) to yield **$Br_2$PD-12** (67.2 mg, 75.0 μmol, 77%) as a purple solid: $^1$H NMR (400 MHz, DMSO-d6) δ 8.47 (s, 1H) 8.42 (d, *J* = 8.3 Hz, 2H), 8.10 (s, 1H), 7.88 (s, 1H), 7.51 (d, *J* = 8.3 Hz, 2H), 5.35 (br. s, 2H), 4.50 (t, *J* = 5.1 Hz, 2H), 4.38 (d, *J* = 6.0 Hz, 2H), 4.30 (s 2H), 3.78 (t, *J* = 5.3 Hz, 2H), 3.51–3.43 (m, 10 H), 3.39 (t, *J* = 6.0 Hz, 2H), 3.18 (q, *J* = 5.9 Hz, 2H), 2.99 (s, 3H), 2.18 (t, *J* = 7.5 Hz, 2H), 2.10 (t, *J* = 7.4 Hz, 2H), 1.76 (quint., *J* = 7.7 Hz, 2H).

### N1-(2-(2-(2-(2-(4-((2-(1-azido-13-oxo-3,6,9-trioxa-12-azapentadecan-15-yl)-4,5-dibromo-3,6-dioxo-3,6-dihydropyridazin-1(2H)-yl)methyl)-1H-1,2,3-triazol-1-yl)ethoxy)ethoxy)ethoxy)ethyl)-N5-(4-(6-methyl-1,2,4,5-tetrazin-3-yl)benzyl)glutaramide ($Br_2$PD-Tz-$N_3$)

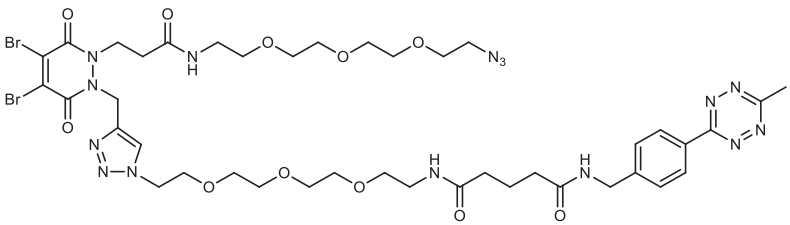

To a solution of 3-(4,5-dibromo-2-((1-(1-(4-(6-methyl-1,2,4,5-tetrazin-3-yl)phenyl)-3,7-dioxo-11,14,17-trioxa-2,8-diazanonadecan-19-yl)-1*H*-1,2,3-triazol-4-yl)methyl)-3,6-dioxo-3,6-dihydropyridazin-1(2*H*)-yl)propanoic acid **$Br_2$PD-12** (40 mg, 45 μmol) in

DCM (2.5 mL) was added, at 21°C, HATU (28.1 mg, 74 μmol), and DIPEA (5.78 mg, 45 μmol), and the reaction stirred for 5 min. Subsequently, to this solution was added at 21°C a solution of 2-(2-(2-(2-azidoethoxy)ethoxy)ethoxy)ethan-1-amine (14.6 mg, 67 μmol) in DCM (2.5 mL), and the resulting solution was stirred at room temperature for 16 h. After this time, the reaction was diluted with EtOAc (10 mL) and washed with sat. aq. $NaHCO_3$ (3 × 10 mL), 1 M HCl (3 × 10 mL), $H_2O$ (10 mL), brine (10 mL), dried ($MgSO_4$), filtered and the solvent removed *in vacuo*. The crude residue was purified by flash column chromatography (0–10% MeOH in DCM) to afford **$Br_2$PD-Tz-$N_3$** (16.7 mg, 15 μmol, 34%) as a purple solid. $^1$H NMR (500 MHz, CDCl3) δ 8.52 (d, *J* = 8.4 Hz, 2H), 7.84 (s, 1H), 7.50 (d, *J* = 8.5 Hz, 2H), 6.74 (br. s, 1H), 6.65 (br. s, 1H), 6.43 (br. s, 1H), 4.65 (t, *J* = 6.8 Hz, 2H), 4.54 (d, *J* = 5.9 Hz, 2H), 4.50 (t, *J* = 4.9 Hz, 2H), 3.85 (t, *J* = 5.1 Hz, 2H), 3.70–3.50 (m, 24 H), 3.41 (td, *J* = 10.3, 5.1 Hz, 6H), 3.09 (s, 3H), 2.66 (t, *J* = 6.8 Hz, 2H), 2.38 (t, *J* = 7.0 Hz, 2H), 2.35 (t, *J* = 7.1 Hz, 2H), 2.01 (quint., *J* = 7.0 Hz, 2 H).

## QUANTIFICATION AND STATISTICAL ANALYSIS

All error bars represent the mean ± standard deviation. In every figure, error bars are not shown if the standard deviation is smaller than the point. All concentrations were measured in triplicates when performing the ELISA assays, as indicated in the figure legend. Initial experiments of the DoE only used replicates for the center point (*N* = 5). Experiments for optimizing the reagent ratio were performed in duplicates, as indicated in the figure legend. Results of the DoE experiments were analyzed using factorial ANOVA using Statistica software. All data fitting and all other statistical analysis were performed using GraphPad Prism software.

No specific method was used to determine whether the data met assumptions of the statistical approach.